



Universidad Autónoma  
de Madrid

**Biblos-e Archivo**  
Repositorio Institucional UAM

**Repositorio Institucional de la Universidad Autónoma de Madrid**  
<https://repositorio.uam.es>

Esta es la **versión de autor** del artículo publicado en:  
This is an **author produced version** of a paper published in:

Chemical Engineering Journal 358 (2021): 1574-1582

**DOI:** <https://doi.org/10.1016/j.cej.2018.10.154>

**Copyright:** © 2019 Elsevier Ltd. This manuscript version is made available under the CC-BY-NC-ND 4.0 licence <http://creativecommons.org/licenses/by-nc-nd/4.0/>

El acceso a la versión del editor puede requerir la suscripción del recurso  
Access to the published version may require subscription

# **C-modified TiO<sub>2</sub> using lignin as carbon precursor for the solar photocatalytic degradation of acetaminophen**

A. Gómez-Avilés\*, M. Peñas-Garzón, J. Bedia, J.J. Rodriguez, C. Bolver

*Sección de Ingeniería Química, Facultad de Ciencias, Universidad Autónoma de Madrid, Campus Cantoblanco, E-28049 Madrid, Spain*

Corresponding author. E-mail address: [almudena.gomeza@uam.es](mailto:almudena.gomeza@uam.es)

## Abstract

This work deals with the removal of emerging pollutants in water by solar light with photocatalysts based on C-modified  $\text{TiO}_2$  materials, using lignin as carbonaceous precursor and acetaminophen as target compound. This provides a way of lignin valorization, a large-scale by-product from the pulp and paper industry and the future lignocellulosic biorefinery. Several C-modified  $\text{TiO}_2$  materials were prepared following a hydrothermal method and a further thermal treatment in different atmospheres (air or nitrogen). The resulting catalysts were fully characterized by different techniques to learn on the structure-photoactivity relation. Complete acetaminophen conversion was achieved after only 1 h under solar irradiation with the photocatalysts calcinated under air atmosphere (C-Ti-400air and C-Ti-500air), being  $\cdot\text{OH}$  and  $\text{O}_2^{\cdot-}$  radicals the main reactive oxygen species involved in the acetaminophen photodegradation. These photocatalysts yielded the highest activity, which was maintained upon four successive uses. These findings are discussed with a focus on the development of active photocatalysts under solar light for the photodegradation of emerging pollutants.

**Keywords:** *Lignin,  $\text{TiO}_2$ , solar photocatalysis, water purification, emerging pollutants.*

## 1. Introduction

In the last decades, there has been an increasing demand on the development of cost-effective technologies capable of dealing with hazardous water pollutants. In this context, photocatalysis can be operated at mild conditions and use only oxygen as primary reagent. There is a current trend towards the use of visible and solar light as renewable and inexpensive energy sources [1,2]. A wide diversity of species has been investigated, like the so-called contaminants of emerging concern (CECs), endocrine disruptors compounds, bacteria and cyanotoxins. CECs are characterized for being not usually monitored species in the environment and whose adverse consequences are newly identified [3]. These compounds include many different groups, such as, pharmaceuticals and personal care products, pesticides, disinfection by-products, wood preservation and industrial chemicals and so on. They are widespread and in general poorly removed in conventional wastewater treatment plants (WWTPs). As a consequence, emerging pollutants are usually found in low concentration in water streams and represent so far a public health problem.

Photocatalysis is based in the ability of semiconductor materials to generate a hole-electron pair ( $h^+e^-$ ) through the jump of an electron from the valence to the conduction band by the action of a photon with enough energy to allow the electron overcome the band gap edge between both bands [4]. Semiconductor photocatalysts promote redox reactions, since electrons act as reducing agents while holes are strong oxidation sites. This promotes photodegradation reactions either directly or indirectly, i.e. through the formation of hydroxyl radicals and other reactive oxygen species (ROS) [5]. Among the different photocatalysts,  $TiO_2$  is still the most widely used due to its well-known advantages: low cost, non-toxicity and chemical stability [6,7]. Nevertheless, the

difficulty of its recovery when using  $\text{TiO}_2$  powder and the relatively limited adsorption capacity and porosity are among the main technological disadvantages. However, probably one of the main drawbacks of  $\text{TiO}_2$  is its lower efficiency under solar irradiation since its band gap requires UV light to allow charge separation. Therefore,  $\text{TiO}_2$  only uses 5% of the solar spectrum to yield the photocatalytic reactions involved in water purification [8]. With the purpose of overcoming those drawbacks, different approaches have been analysed in the literature to enhance the activity of  $\text{TiO}_2$  under solar light, such as, self-structural modifications [9], doping (metal and non-metal), noble metal loading and surface sensitization [2,10,11].

Structural modifications of  $\text{TiO}_2$  with carbon have been described as a promising way to enhance the titania activity under visible radiation [12]. Some works described the synthesis of C- $\text{TiO}_2$  nanoparticles and films where the carbon substitutes the oxygen lattice of  $\text{TiO}_2$  resulting in the formation of oxygen vacancies [13,14]. The formation of Ti-C bonds and the presence of C as substitutional and interstitial lattice sites have been also reported, their formation depending on the synthesis route [15]. Although these species can act as trap centers, enhancing the photocatalytic activity, their presence in high concentrations can have some inhibitory effects [16]. It has been reported that the synthesis method affects to the activity of the resulting C-modified  $\text{TiO}_2$ . These methods include sol-gel modified with carbon precursors, treatment with gaseous carbon sources, flame pyrolysis of Ti metal, thermal oxidation of TiC and carbonization of organic templates [17]. However, there is no a simple way to obtain C- $\text{TiO}_2$  with high photoefficiency. Some drawbacks of these approaches to enhance the  $\text{TiO}_2$  activity include aggregation of carbon species and distortion of the  $\text{TiO}_2$  lattice, thus favoring undesired electron-hole recombination [18].

The current study deals with the hydrothermal synthesis of C-modified TiO<sub>2</sub> photocatalysts using lignin as carbonaceous precursor. This approach provides a way of lignin valorization, a large-scale by-product from the pulp and paper industry with high growth expectations from the future lignocellulosics-based biorefinery. Hydrothermal synthesis has been used because it allows obtaining titania nanotubes with a fairly well-developed surface area [19,20]. Although this process has been reported in the literature, to the best of our knowledge there are no studies on the C-modified titania derived from these nanotubes. The C-modified TiO<sub>2</sub> photocatalysts have been tested for the degradation of a model pharmaceutical (acetaminophen) in water under solar irradiation.

## **2. Experimental**

### **2.1. Materials**

Lignin was supplied by LignoTech Iberica, Spain. Titanium (IV) isopropoxide (TIP, > 97%) was purchased from Sigma Aldrich. Ethanol (96%), NaOH (pharma grade) and HCl (37%) were purchased from Panreac. Acetaminophen (ACE) (> 99%, Sigma Aldrich) was selected as model compound for testing the photocatalytic activity. For preparing the mobile phase for liquid chromatography, acetonitrile and formic acid (>95%) were purchased from Panreac and Sigma Aldrich, respectively. KI (99%) and 1,4-benzoquinone (> 98%) were both purchased from Sigma Aldrich, while isopropanol (99.7%) and AgNO<sub>3</sub> (> 99%) were supplied by Panreac and Alfa Aesar, respectively. Deionized and doubly distilled water was used throughout this work.

### **2.2. Synthesis of the catalysts**

Firstly,  $\text{TiO}_2$  was prepared by sol-gel following the methodology reported by Maira et al. [21,22]. In summary, 1 mL of titanium isopropoxide (TIP) was dropped into a well-mixed water/isopropanol solution (vol. ratio 1/2) under stirring for the TIP hydrolysis. The  $[\text{H}_2\text{O}]/[\text{TIP}]$  ratio was fixed at 4. Following the sol-gel procedure, the final solid was dried at room temperature for 1 h and finally heated at 450 °C in air for 3 h in order to transform the amorphous solid to the crystalline titania. This  $\text{TiO}_2$  was used as raw material. Further, in a typical synthesis, 1 g of  $\text{TiO}_2$  and 0.5 g of lignin (weight ratio 0.5) were suspended in 75 mL of a 10 M solution of NaOH under magnetic stirring for 10 minutes following another 10 minutes in a sonication bath. Other lignin to  $\text{TiO}_2$  weight ratios (0.1-1.0) were previously checked before selecting the above mentioned as the optimum. The suspension was charged into a Teflon-lined autoclave and subjected to hydrothermal treatment at 130 °C for 48 h. The resulting brown solid was separated from the solution by centrifugation (5000 rpm, 5 min), washed several times with 0.3 N aqueous HCl and then rinsed with distilled water until neutral pH. Finally, it was dried in an oven at 60°C overnight and denoted as C-Ti. The same procedure was used for  $\text{TiO}_2$  without lignin obtaining a carbon-free sample denoted as Ti. This last was calcined in air ( $150 \text{ Ncm}^3 \cdot \text{min}^{-1}$ ) in a horizontal tube furnace at 300, 400 and 500 °C for 2 h. The best results in terms of ACE conversion were obtained with the sample calcinated at the highest temperature (named Ti-500air) which was the only one included in the study. The C-Ti sample was treated in the same tube furnace for 2 h under air flow ( $150 \text{ Ncm}^3 \cdot \text{min}^{-1}$ ) at 300, 400 or 500 °C and under  $\text{N}_2$  flow ( $150 \text{ Ncm}^3 \cdot \text{min}^{-1}$ ) at 500 and 750 °C, yielding the samples denoted as C-Ti-300air, C-Ti-400air, C-Ti-500-air, C-Ti-500 $\text{N}_2$  and C-Ti-750 $\text{N}_2$ .

### 2.3. Characterization techniques

X-ray diffraction (XRD) profiles were obtained in a Bruker D8 diffractometer equipped with a Sol-X energy dispersive detector operating with Cu K $\alpha$  radiation. The XRD patterns were collected from 2 to 70° of 2 $\theta$  at a scanning rate of 1.5°/min to study the structure. The average crystal size (D) was estimated using the Scherrer's equation from the most intense diffraction peak (101) of anatase phase. Elemental analyses were carried out in a LECO CHNS-932 apparatus to determine C, N, S and H contents. N<sub>2</sub> adsorption-desorption isotherms at -196 °C were obtained in a Micromeritics TriStar 123 equipment. Before analysis, the samples were degassed under vacuum at 150 °C overnight. The specific surface area was calculated from the BET method, while the external or non-microporous surface area (S<sub>EXT</sub>) was estimated from the t-plot method of De Boer. The total pore volume (V<sub>T</sub>) corresponds to the amount of nitrogen adsorbed up to 0.99 relative pressure. UV–vis diffuse reflectance spectra (DRS) were collected in the 250-800 nm region with a Shimadzu 2501PC UV–vis spectrophotometer equipped with an integrating sphere, using BaSO<sub>4</sub> as reference material. The band gap energy (E<sub>g</sub>) was estimated from the reflectance spectrum by the Tauc plot method [23], considering an indirect semiconductor for the TiO<sub>2</sub> [24] and following the equation  $\alpha h\nu = \alpha_0 (h\nu - E_g)^{1/2}$ , where  $\alpha$ ,  $h$ ,  $\nu$  and  $E_g$  are the absorption coefficient, Plank constant, light frequency and the energy gap of a semiconductor, respectively. This method uses a plot of  $(\alpha h\nu)^{1/2}$  vs  $h\nu$  that results in a curve whose linear branch is extrapolated to the X axis and its interception provides the band gap value. Transmission electron microscopy (TEM) images were obtained using a Tecnai G220 microscope (FEI COMPANY) at an accelerating voltage of 200 kV. X-Ray photoelectron spectroscopy (XPS) was used to analyze the surface elemental composition of some catalysts. The XPS spectra were obtained with a K-Alpha-Thermo Scientific spectrometer (Waltham, MA, USA) using Al K $\alpha$  X-ray (1486.68 eV) as excitation source. The C1s peak was set at 284.5 eV and



used as internal reference to locate the other peaks. The fitting of the XPS signals was made by the least-squares method using peaks with Gaussian–Lorentzian shapes.

#### 2.4. Photocatalytic degradation tests

The solar photocatalytic degradations of acetaminophen were performed in a batch Pyrex glass reactor, with magnetic stirring placed inside a Suntest simulator (Suntest XLS+ photoreactor, ATLAS) equipped with a 765 - 250 W·m<sup>-2</sup> Xe lamp (61 - 24 W·m<sup>-2</sup> from 300 to 400 nm,  $5.5 \cdot 10^{19}$  -  $1.4 \cdot 10^{20}$  photons·m<sup>-2</sup>·s<sup>-1</sup>) and a “Daylight” filter (cuts off 290 nm), which simulates solar radiation. The intensity of irradiation was fixed at 600 W·m<sup>-2</sup> (107.14 klx). The reaction temperature was monitored and reached a constant value of  $38 \pm 1$  °C after the first 20 min of irradiation. In a typical experiment, the catalyst (250 mg·L<sup>-1</sup>) was dispersed in an aqueous solution containing 5 mg·L<sup>-1</sup> of acetaminophen (>99% Sigma Aldrich). The dispersion was left under stirring in dark for 1 h to achieve the adsorption equilibrium. Then, the light was connected, and the reactor was exposed to solar irradiation for 4 h. At given time intervals, 400 µL of the suspension were collected and the photocatalyst was removed by filtration using PTFE syringeless filters (Whatman 0.2 µm). The liquid phase was analysed by HPLC (Varian Pro-Start 310) with diode array detector (330 PDA) and a reversed phase C18 column (Eclipse Plus 5 µm, Agilent). A mixture of acetonitrile/formic acid 0.1% v/v (Panreac, >95% Sigma Aldrich, respectively) (gradient method: 10/90–40/60%) was used as the mobile phase, with a constant flow of 0.35 mL/min. The detection wavelength for acetaminophen was set at 256 nm, according to the UV–vis absorption spectrum previously recorded for this compound. All the photocatalytic degradation experiments were performed in triplicate and the corresponding confidence intervals at 95% of significance were calculated.

The experiments with scavengers were performed following the same conditions described above. The scavenger was added to the acetaminophen solution prior to the switch on the light. The concentration of the scavenger was fixed to 0.06 M in each case. Isopropanol, benzoquinone, KI and AgNO<sub>3</sub> were selected as radical scavengers. The reaction was followed taking aliquots at different times and the acetaminophen concentration was analyzed with the same chromatographic method.

### **3. Results and discussion**

#### **3.1. Characterization**

Figure 1 shows the diffraction patterns of the Ti and C-Ti samples obtained from hydrothermal synthesis as well as the resulting from the different further heat treatments of those materials. The Ti and C-Ti diffractograms are very similar, with peaks centered at  $2\theta = 24.4, 27.7$  and  $48.3^\circ$ , which can be associated to the formation of titanate nanotubes similar to those reported in literature [19,20]. Further thermal treatment of these nanotubes provokes substantial modifications of their structure. Calcination in air at 300 °C maintained the original structure of nanotubes, which changed by increasing the temperature to 400 °C. The C-Ti-400air and C-Ti-500air samples show the characteristic peaks associated to the crystallization of anatase phase (JCPDS–78–2486). It is noteworthy that the C-Ti-500air sample appears less crystalline than the Ti-500air sample synthesized without lignin, suggesting that the incorporation of this carbon precursor affects to anatase crystallization. The air treatment allowed anatase formation but the elemental chemical analyses (Table 1) revealed a low carbon content (0.3 and 0.1% for C-Ti-400air and C-Ti-500air respectively), as a consequence of the carbon combustion under those conditions. Thus, additional samples were obtained upon thermal treatment but in N<sub>2</sub> atmosphere at 500 and 750 °C. The XRD pattern of C-

Ti-500N<sub>2</sub> sample depicts the characteristic peaks of anatase phase, apparently with lower crystallinity than C-Ti-500air. As expected, the solid contains a higher C amount (Table 1), ca. to 5.8%. The thermal treatment under N<sub>2</sub> at 750 °C allowed also maintaining some C content in the resulting solid although lower than when treated at 500 °C (ca. to 3%) consistently with a higher loss of C-containing volatile matter at increasing temperature. Furthermore, at this temperature, the TiO<sub>2</sub> structure changes and rutile phase (JCPDS-21-0276) appears next to the anatase phase. The crystal size of the anatase phase, as estimated by the Scherrer's equation, is included in Table 1. As can be seen, the incorporation of lignin reduces the crystal size of the anatase phase, except in the case of C-Ti-750N<sub>2</sub>. Carbon must be doping the anatase structure as substitutional anion and/or interstitial cation [25].

**Figure 1.** XRD patterns of Ti and C-Ti samples from hydrothermal synthesis and the resulting from further heat treatment under different conditions.

**Table 1.** C, H, N content and average crystal size of the synthesized photocatalysts.

Figure 2 shows N<sub>2</sub> adsorption-desorption isotherms of the synthesized catalysts. All of them belong to type IV of the IUPAC classification [26], characteristic of mesoporous materials, as suggest the adsorption of N<sub>2</sub> at medium-high relative pressures and the presence of H3 type hysteresis loops. The hydrothermal treatment yielded titania nanotubes (Ti sample) with a well-developed porous texture, showing significantly higher N<sub>2</sub> adsorption than the calcined sample (Ti-500air) within the whole range of relative pressure. The thermal treatment results in a loss of nanotube structure (as shown by XRD). Including lignin as carbon source in the hydrothermal synthesis did

not affect significantly the porous texture of the resulting carbon-modified titania nanotubes (C-Ti sample), as can be seen from Figure 1 and Table 2. Upon calcination at 300 °C the porous texture is still conserved, but increasing that temperature provokes a decay of surface area, consistent with the loss of tubular structure observed by XRD. Thermal treatments in N<sub>2</sub> atmosphere led also to a loss of surface area, less pronounced than upon air calcination at 500 °C, which can be attributed to the significantly different amount of carbon (char) fraction in both samples in addition to the different crystal size of the anatase phase (Table 1). Increasing the temperature to 750 °C provokes a quite significant loss of porosity although with somewhat more relative contribution of microporosity consistent with the lower amount of carbon fraction but more deeply devolatilized. Also, increasing the temperature of the heat treatment up to 750 °C results in a higher crystallinity of the sample, affecting to the surface area. All the samples are essentially mesoporous, as can be seen from the values of total ( $S_{\text{BET}}$ ) and external or non-microporous ( $S_{\text{EXT}}$ ) surface area in Table 2. The loss of surface area upon thermal treatment is due to the transformation of titanate nanotubes into anatase phase. It must be remarked that these materials have high surface area values than other conventional TiO<sub>2</sub> anatase [17].

**Figure 2.** N<sub>2</sub> adsorption-desorption isotherms of the synthesized

**Table 2.** Porous texture and band gap values ( $E_g$ ) of the photocatalysts.

The morphology of the samples was analyzed by TEM. Representative images are depicted in Figure 3. As can be seen in Figure 3A (Ti sample) the hydrothermal synthesis yields a homogeneous nanotube morphology in agreement with previous

works with P25 [19,27]. The nanotubes show sizes close to 10 nm of diameter and lengths of 100 nm or more. The addition of lignin in the hydrothermal synthesis yields likewise a nanotube morphology (Figure 3B, C-Ti). However, in this case, the wall of the nanotubes seems to present a certain rugosity probably as a consequence of the presence of a carbon coating in the nanotubes [28]. This modification of the morphology is expected to have some influence in the photocatalytic activity of these materials under solar light. TEM images of the calcined samples (Figures 3C and D) show a very significant effect on the morphology of the samples. As can be seen, the nanotube morphology is lost during the calcination treatment at 500 °C. This is in agreement with the structural transformation observed by XRD, where the titanate nanotubes disappeared while crystallizing the anatase structure. After calcination, the samples show a lobular morphology with particle sizes in the range of 20 to 30 nm and absence of titania nanotubes. Therefore, the calcination process provokes important structural changes in the Ti-based nanotubes with significant impact on the porosity and morphology of the samples.

**Figure 3.** TEM images of (A) Ti, (B) C-Ti, (C) Ti-500air and (D) C-Ti-500air.

Table 3 summarizes the surface elemental composition of Ti-500air, C-Ti-500air and C-Ti-500N<sub>2</sub> photocatalysts as obtained by XPS. Only C, Ti and O were detected. As expected, the highest amount of carbon (27.4 wt.%) corresponds by far to the sample treated in N<sub>2</sub> at 500 °C (C-Ti-500N<sub>2</sub>), consistently with the results of elemental analyses (Table 1). However, it is noticeable the amount of C of Ti-500air, where no carbon source was added in the synthesis, and even C-Ti-500air, where carbon had been removed by calcination according to elemental analysis. This presence of adventitious

carbon on the surface of these samples is due to a layer of carbonaceous material usually found on the surface of most air exposed samples, probably in form of adsorbed CO<sub>2</sub>. The atomic O/Ti ratio is approximately 2.3, not far from 2.0 the theoretical ratio for TiO<sub>2</sub>. Figure 4 shows the C 1s, Ti 2p and O 1s XPS high resolution spectra of Ti-500air, C-Ti-500air and C-Ti-500N<sub>2</sub> photocatalysts. The analysis of the C 1s spectra shows three different peaks, one with the highest intensity, centered at 284.5 eV and the other two at around 288.5 and 289.2 eV. The first is associated to C-C bonds. The intensity of this peak is clearly higher for the sample with the higher amount of carbon (C-Ti-500N<sub>2</sub>). This carbon can act as photo-sensitizer increasing the activity of the photocatalyst under solar or visible light [29,30]. The second peak, located at approximately 288.5 eV, is the characteristic shake-up line for carbon from the  $\pi \rightarrow \pi^*$  transition. Finally, the last peak centered at around 289.2 eV and only observed in C-Ti-500N<sub>2</sub>, could be associated to the presence of Ti-O-C carbon bonds. The formation of these bonds can be related to the presence of C atoms as interstitial cations [25], corroborating the incorporation of doping C into the TiO<sub>2</sub> lattice and the reduction of the average crystal size described before by XRD. It is also worth mentioning the absence of the peak related to Ti-C bonds at 281.0 eV [31]. This absence suggests that C does not substitute O in the TiO<sub>2</sub> lattice. The type of substitution of the carbon atoms in the TiO<sub>2</sub> lattice seems to be highly dependent on the type of doping since different behaviors have been reported in the literature [32-34].

**Table 3.** Surface elemental composition (at., %) of the photocatalysts as obtained by XPS.

**Figure 4.** C 1s, Ti 2p and O 1s XPS high-resolution spectra of Ti-500air, C-Ti-500air and C-Ti-500N<sub>2</sub>.

The high resolution Ti 2p XPS spectra of the different photocatalysts (Figure 4) show two peaks at around 458.5 and 464.2 eV ascribed to Ti 2p<sub>3/2</sub> and Ti 2p<sub>1/2</sub>, respectively. These peaks correspond to the typical signal of Ti<sup>4+</sup> oxidation state, with the standard line separation between Ti 2p<sub>3/2</sub> and Ti 2p<sub>1/2</sub> of 5.2 eV [35], in agreement with the TiO<sub>2</sub> lattice of anatase phase. It can be observed that the calcination treatment in air results in a slight displacement of the Ti 2p spectrum to lower binding energies. This behaviour suggests the formation of oxygen vacancies and/or Ti<sup>3+</sup> defects [31], probably during the removal of carbon by combustion. In contrast, the introduction of C atoms in the TiO<sub>2</sub> lattice and the subsequent thermal treatment in N<sub>2</sub> atmosphere results in a displacement of the Ti 2p signal to higher binding energies. This positive shift of the binding energy has been previously observed in other studies and has been ascribed to the generation of lattice distortions due to the inclusion of C atoms into the TiO<sub>2</sub> lattice [36,37]. Very similar behaviours are observed when comparing the high-resolution O 1s spectra of Figure 4. Taking as reference the binding energy values of Ti-500 air sample, the O 1s spectrum shows a peak centered at 529.6 eV and associated to O atoms bonded to Ti in the TiO<sub>2</sub> lattice. The introduction of C atoms in the lattice and their subsequent removal by combustion during the calcination step results again in a displacement of the O 1s spectrum to lower binding energies, probably due to the formation of oxygen vacancies [36,38]. On the other hand, the treatment in N<sub>2</sub> results in a C-modified TiO<sub>2</sub> giving rise to displacement of the O 1s signal to higher binding energies.

The UV-vis DRS absorption spectra of the synthesized photocatalysts are depicted in Figure 5A. Ti sample displayed an absorption edge close to 400 nm similar to that of other titanate nanotubes [39]. The addition of lignin in the hydrothermal treatment (C-Ti

sample) leads to an absorption edge red-shifted, respect to that of the Ti sample, and light absorption in the visible region ( $> 400\text{nm}$ ) due to lignin-derived carbon material, which is also responsible of the brown color of that sample. Upon calcination of C-Ti in air at  $300\text{ }^{\circ}\text{C}$ , the absorption edge shifted to a lower wavelength and the absorption in the visible range decreased due to partial combustion of the carbonaceous material. This effect was more evident at higher calcination temperatures. Carbon was almost completely removed (see carbon contents in Table 1) and the resulting C-Ti-400air and C-Ti-500air samples displayed the absorption edge at  $390\text{ nm}$ , analogous to that of  $\text{TiO}_2$  anatase [40]. The UV-vis DRS spectra of the samples heat-treated in  $\text{N}_2$  atmosphere at  $500$  and  $750\text{ }^{\circ}\text{C}$  show absorption edges shifted to the red spectral region compared with the C-Ti sample, but their high absorption in the visible region overlapped the edge. These samples have a black colour caused by the presence of carbon (see C content in Table 1) which is the responsible of the light absorption at wavelengths in the visible region. The samples were further characterised by UV-vis DRS at reflectance mode in order to estimate the band gap values, except for the samples heated under  $\text{N}_2$ , where the black color did not allow to estimate the band gap value of the titania phase. The band gap energy ( $E_g$ ) can be calculated from the UV-vis spectrum using the Tauc Plot method by analysing the linear relationship between  $(\alpha h\nu)^{1/2}$  and photon energy  $h\nu$ . In these plots the  $E_g$  values are obtained from the intercept of the extrapolation of the linear branch with the abscissa (Figure 5B). The resulting values are included in Table 2. The band gap energy of Ti is  $3.25\text{ eV}$  analogous to other titania samples [39] while the coloured C-Ti yielded a lower band gap,  $2.95\text{ eV}$ , due to the presence of lignin-derived carbonaceous material. The band gap energies of C-Ti-300air, C-Ti-400air and C-Ti-500air are  $3.28$ ,  $3.25$  and  $3.18\text{ eV}$ , respectively, characteristic of  $\text{TiO}_2$  materials.



**Figure 5.** (A) UV–vis diffuse reflectance spectra and (B) the  $(\alpha h\nu)^{1/2}$  versus  $(h\nu)$  plot of the synthesized photocatalysts

### 3.2. Photocatalytic degradation of acetaminophen using solar light

Figure 6 represents the evolution of the acetaminophen concentration versus time under solar irradiation with the synthesized photocatalysts. In the absence of photocatalyst (photolysis blank test, results not shown), the concentration of acetaminophen remained constant along 6 h of solar irradiation, so that acetaminophen can be considered stable under solar light in absence of photocatalyst. The amount of acetaminophen adsorbed on the different photocatalysts without light irradiation can be considered negligible (lower than 6%) despite the differences in surface area of the samples. From the results of Figure 6 it can be seen that the C-modified titania nanotubes, C-Ti, show a significantly higher activity than the non-modified ones (Ti), probably because of a sensitization of  $\text{TiO}_2$  by the carbon material. However, conversion of acetaminophen remained below 70 % after 4 h of illumination. Probably, the absence of a well-defined crystal structure of anatase is responsible of this relatively low photoactivity since it is well known that amorphous titania is not photoactive [41]. Calcination in air at temperature somewhere above 300 °C had a dramatic beneficial effect on the activity of the C-Ti catalyst, so that the samples calcined at 400 and 500 °C allowed complete conversion of acetaminophen in only 1 h of reaction time. This can be explained by the crystallization of  $\text{TiO}_2$  into anatase (with a band gap energy of 3.12 eV), which is the most active titania phase in photocatalytic applications [42,43]. At the lowest calcination temperature tested (300 °C) there is no significant crystallization of anatase, the solid maintaining still the nanotube structure (see Figure 1). Thus, the high photoactivity of the samples calcined at higher temperature can be attributed to anatase

crystallization with a small crystal size (11.8 nm, Table 1). The removal of C atoms from the TiO<sub>2</sub> lattice upon combustion would give rise to vacancies and/or defects (substitutional or interstitial) as suggested by the XPS results. The effects caused by the presence of vacancies and/or defects in C-modified TiO<sub>2</sub> has been reported in the literature, to improve the photoactivity under visible light because they can act as trap centers [13,16], as supported by the highest conversions obtained with C-Ti-400air and C-Ti-500air than with Ti-500air. Increasing the calcination temperature from 400 to 500 °C did not produce any further improvement of the photocatalytic activity. Thermal treatment in N<sub>2</sub> atmosphere reduced the activity of the resulting samples, even for the one with the smallest crystal size (C-Ti-500N<sub>2</sub>). These materials maintain much more carbon than the ones calcined in air (see Table 3 for surface C content), which favors a high light absorption diminishing the photocatalytic efficiency.

**Figure 6.** Time-course of acetaminophen concentration under solar irradiation with the synthesized photocatalysts (250 mg·L<sup>-1</sup> of catalyst; initial acetaminophen concentration: 5 mg·L<sup>-1</sup>; intensity of irradiation: 600 W·m<sup>-2</sup>).

The disappearance of acetaminophen under solar light with the catalysts tested follows quite well a pseudo-first order rate equation. The values of the corresponding rate constant, *k*, are depicted in Figure 7. The highest values, corresponding to C-Ti catalysts calcined in air at 400 and 500 °C (approximately 3.5 and 4.0 h<sup>-1</sup>, respectively), are much higher than those previously reported by our research group for the solar photocatalytic degradation of phenol (0.15 h<sup>-1</sup>) and rhodamine B (0.66 h<sup>-1</sup>) with Ce-doped and non-doped TiO<sub>2</sub>/clay heterostructures [44,45] or for antipyrine with Zr-doped TiO<sub>2</sub> supported on delaminated clay photocatalysts (0.58 h<sup>-1</sup>) [46]. We also reported on the photodegradation of several pharmaceuticals under solar light with ZnO/sepiolite

heterostructures. The maximum values of the pseudo first-order rate constant were 0.13, 0.19 and 0.38 h<sup>-1</sup> for the disappearance of antipyrine, acetaminophen and ibuprofen, respectively [47], also much below than the obtained with the best photocatalysts described in the current work. Regarding the properties of the C-TiO<sub>2</sub> materials prepared, it is noteworthy that the structural defects caused by the C incorporation (as substitutional anion and/or interstitial cations) are the responsible of the photocatalytic activity of these materials, acting as trap centers of the photogenerated charges.

**Figure 7.** Apparent first order rate constant for acetaminophen disappearance.

The role of the main reactive oxygen species has been investigated using selected scavengers. Figure 8 depicts the values of the first order rate constant with C-Ti-500air catalyst for the acetaminophen degradation under different conditions. Isopropanol has been selected as  $\cdot\text{OH}$  scavenger [48]. When it was added, the degradation rate was reduced considerably. Since  $\cdot\text{OH}$  radicals are very reactive, their reduction by the scavenger inhibited the degradation rate, indicating that the  $\cdot\text{OH}$  radicals are involved in the acetaminophen degradation. The benzoquinone (BQ) has the ability to trap  $\text{O}_2^{\cdot-}$  radicals [48,49]. The BQ addition causes the inhibition of the acetaminophen degradation, as shown in Figure 8. The degradation rate was almost suppressed demonstrating the participation of  $\text{O}_2^{\cdot-}$  in the photodegradation process. It is noteworthy that the  $\text{O}_2^{\cdot-}$  participation has been described in literature. Some references mentioned that the  $\text{O}_2^{\cdot-}$  radicals attacked preferentially organic compounds with aromatic rings (as aromatic ring of ACE) [50,51]. On the other hand, AgNO<sub>3</sub> was used as electron scavenger [51]. Its incorporation reduces the rate constant by almost half indicating that electrons also participate in the process. KI was also chosen as hole-capturer [51]. Its

addition caused a small decrease of the  $k$  value, so although the amount of holes influenced the degradation rate its participation in the reaction is less than the radicals mentioned above. In general terms it could be affirmed that the main reactive oxygen species involved in the acetaminophen photodegradation were  $\cdot\text{OH}$  and  $\text{O}_2\cdot^-$  radicals.

**Figure 8.** Apparent first order rate constant of acetaminophen degradation with C-Ti-500air in presence of different scavengers ( $[\text{ACE}]=5\text{ mg}\cdot\text{L}^{-1}$ ;  $[\text{scavenger}]=0.06\text{ M}$ ;  $[\text{photocatalyst}]=250\text{ mg}\cdot\text{L}^{-1}$ ; intensity of irradiation:  $600\text{ W}\cdot\text{m}^{-2}$ ).

The stability of the photocatalysts is a crucial issue regarding potential application. Figure 9 displays the evolution of the acetaminophen concentration vs irradiation time upon four consecutive cycles with the C-Ti-500air catalyst. After each use the catalyst was filtered, rinsed with distilled water and dried at  $80\text{ }^\circ\text{C}$ . The values of  $k$  for each cycle are included. The results suggest a fairly good performance of the catalyst with no significant loss of activity upon the fourth successive cycles. However, more conclusive long-term experiments under continuous operation need to be carried out in the next future to assess the stability of this promising catalyst upon time on stream.

**Figure 9.** Performance of the C-Ti-500air photocatalyst upon successive cycles (same conditions than in Figure 6).

#### 4. Conclusions

Lignin has been used as carbonaceous precursor to modify the  $\text{TiO}_2$  anatase lattice following a hydrothermal procedure and a subsequent thermal treatment. The hydrothermal synthesis led to the formation of carbon-titania nanotubes with fairly high surface area and essentially mesoporous texture. Further thermal treatment allowed the

transformation of those nanotubes into anatase phase of small crystal sizes, associated to the formation of defects, and relatively high surface area compared with the commonly found for anatase. When the thermal treatment was performed under inert atmosphere gave rise to materials with much higher carbon content, maintaining the anatase phase and small crystal size, but dark color, provoking a great light absorption that diminish its photocatalytic activity. Therefore, the photocatalysts prepared upon calcination in air atmosphere at 400 and 500 °C (C-Ti-400air and C-Ti-500air) were the most active for the photodegradation of acetaminophen, allowing complete in 1 h under solar light. The disappearance of acetaminophen follows a pseudo-first order kinetics with significantly higher values of the apparent rate constants (k) than the reported for some other photocatalysts. The main reactive oxygen species involved in the acetaminophen photodegradation were  $\cdot\text{OH}$  and  $\text{O}_2^{\cdot-}$  radicals, with an inferior contribution of electrons. The best catalysts showed a fairly good stability upon four successive cycles.

## Acknowledgements

The authors acknowledge the financial support from Spanish MINECO (project CTQ2016-78576-R). M. Peñas-Garzón is indebted to Spanish MECD for FPU16/00576 predoctoral contract. We also thanks to Dr. Gamarra and the SAIUEx service for performing the TEM analyses.

## References

**Table 1.** C, H, N content and average crystal size of the synthesized photocatalysts.

Sample	%C	%H	%N	Average crystal size (nm) <sup>a</sup>
Ti-500air	---	---	---	21.7

C-Ti-300air	2.31	1.39	0.08	---
C-Ti-400air	0.32	0.77	0.04	11.8
C-Ti-500air	0.12	0.43	0.00	17.0
C-Ti-500N <sub>2</sub>	5.85	0.79	0.04	11.0
C-Ti-750N <sub>2</sub>	2.97	0.17	0.03	29.6

<sup>a</sup> Anatase crystal size estimated from (101) reflection peak

**Table 2.** Porous texture and band gap values (E<sub>g</sub>) of the photocatalysts.

Sample	S <sub>BET</sub> (m <sup>2</sup> ·g <sup>-1</sup> )	S <sub>EXT</sub> (m <sup>2</sup> ·g <sup>-1</sup> )	V <sub>pore</sub> (cm <sup>3</sup> ·g <sup>-1</sup> )	E <sub>g</sub> (eV)
Ti	327	309	1.20	3.25
Ti-500air	106	100	0.54	3.12
C-Ti	342	329	1.13	2.95
C-Ti-300air	323	300	1.29	3.28
C-Ti-400air	147	138	0.87	3.25
C-Ti-500air	111	102	0.90	3.18
C-Ti-500N <sub>2</sub>	195	195	0.90	---
C-Ti-750N <sub>2</sub>	73	56	0.34	---

**Table 3.** Surface elemental composition (at., %) of the photocatalysts as obtained by XPS.

Muestra	%Ti	%O	%C	O/Ti
Ti-500air	28.3	63.4	8.3	2.24
C-Ti-500air	28.5	63.9	7.8	2.24
C-Ti-500N <sub>2</sub>	21.7	50.9	27.4	2.35

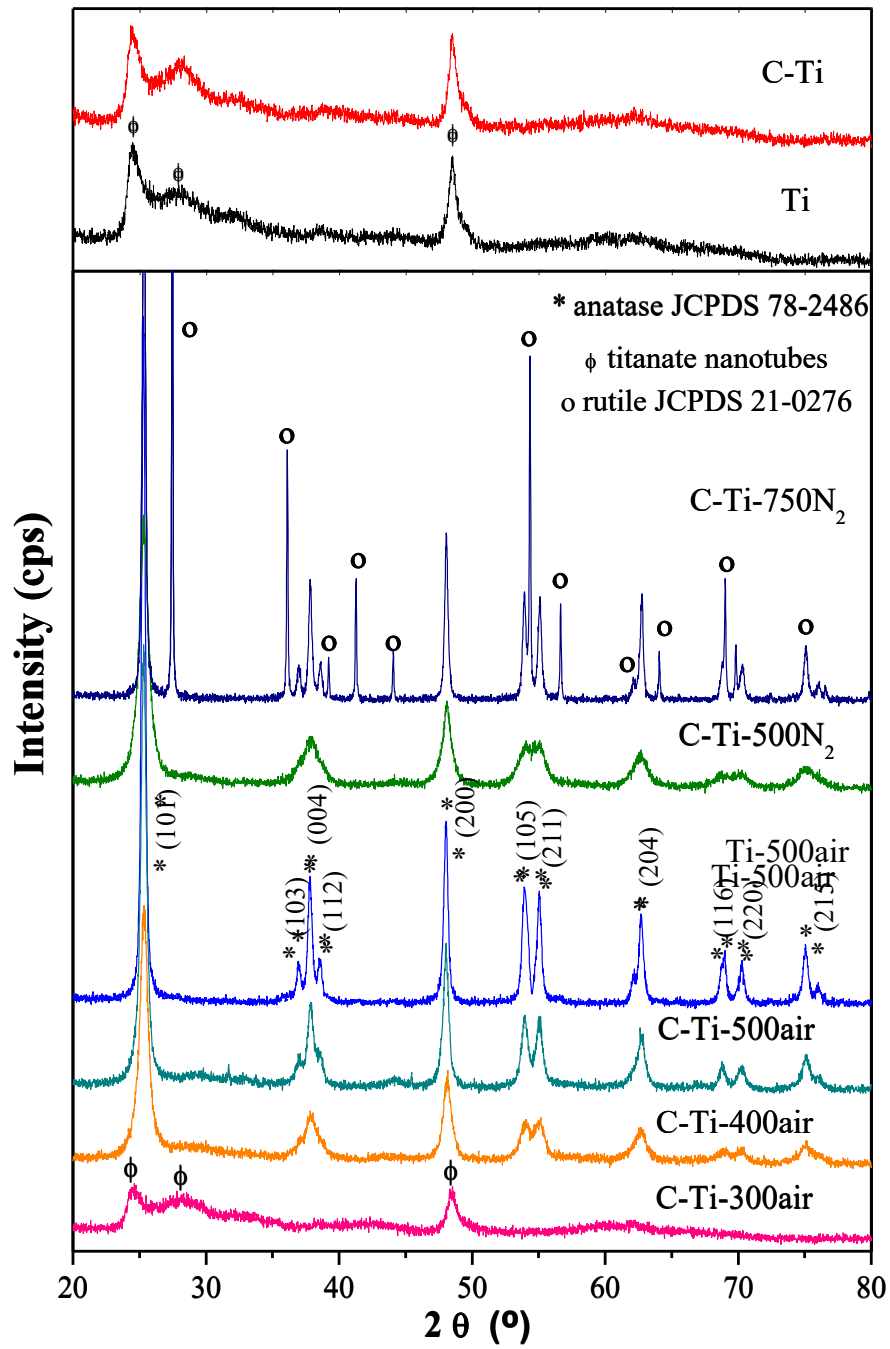


**Figure 1.** XRD patterns of Ti and C-Ti samples from hydrothermal synthesis and the resulting from further heat treatment under different conditions.

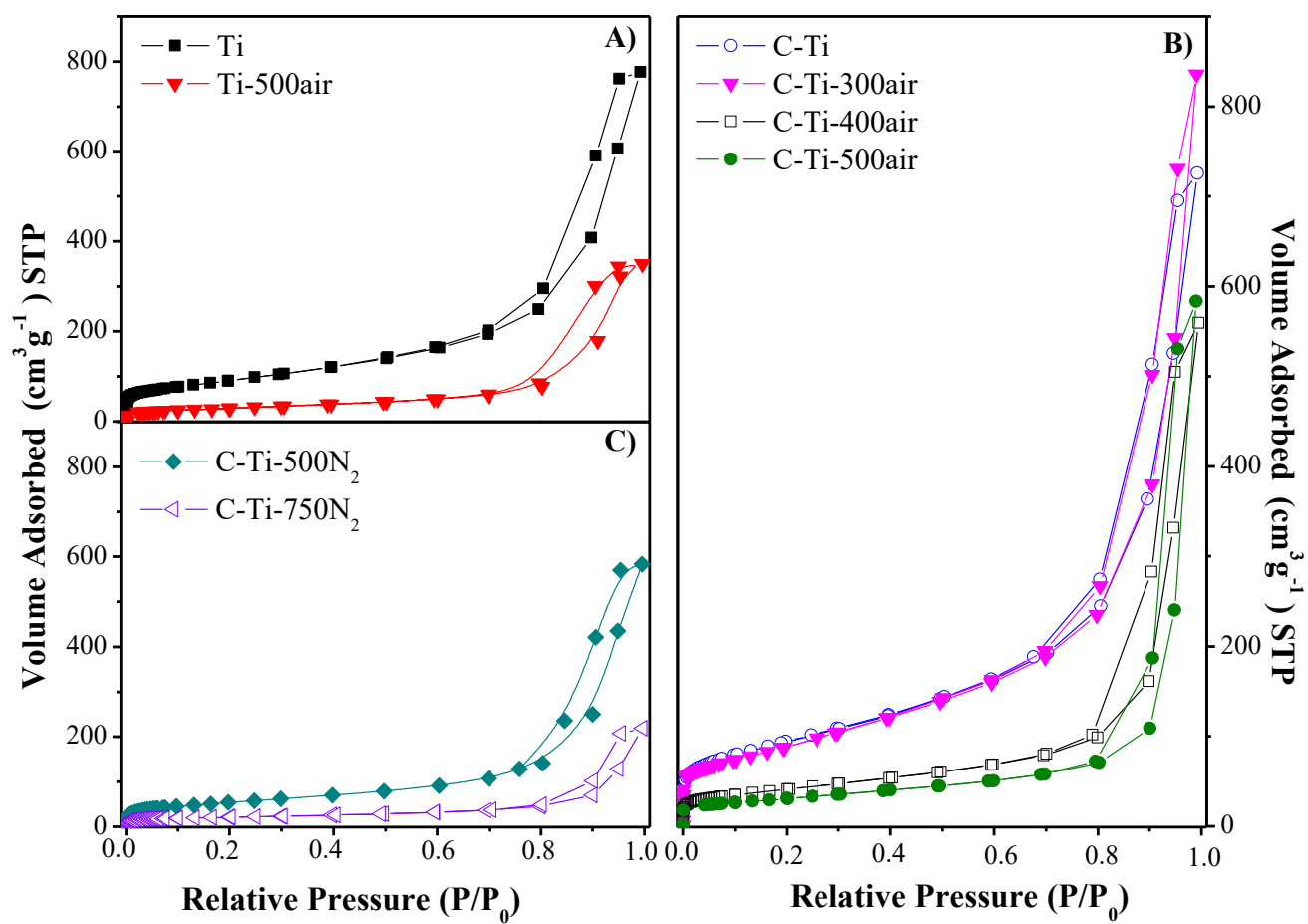


**Figure 2.**  $N_2$  adsorption-desorption isotherms of the synthesized photocatalysts



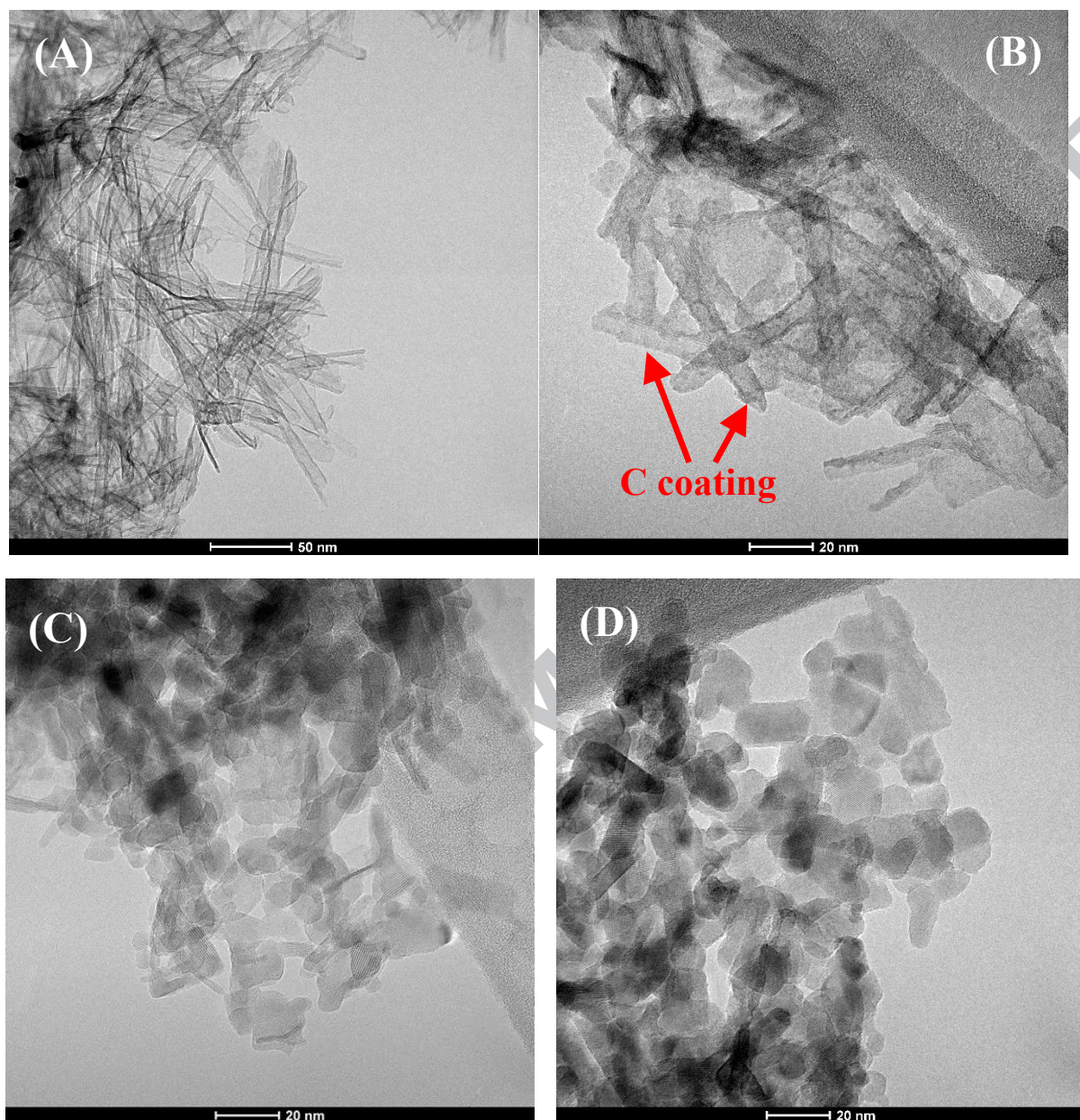


**Figure 3.** TEM images of (A) Ti, (B) C-Ti, (C) Ti-500air and (D) C-Ti-500air

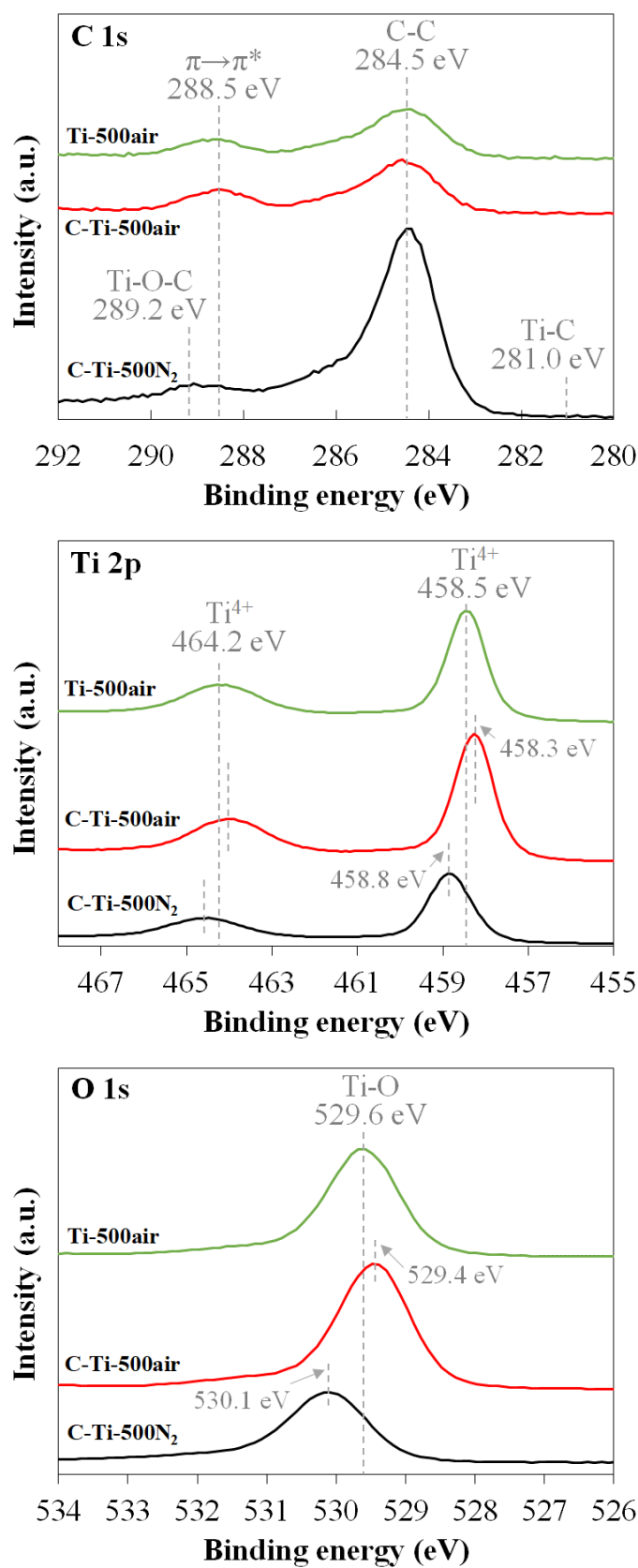


**Figure 4.** C 1s, Ti 2p and O 1s XPS high-resolution spectra of Ti-500air, C-Ti-500air and C-Ti-500N<sub>2</sub>

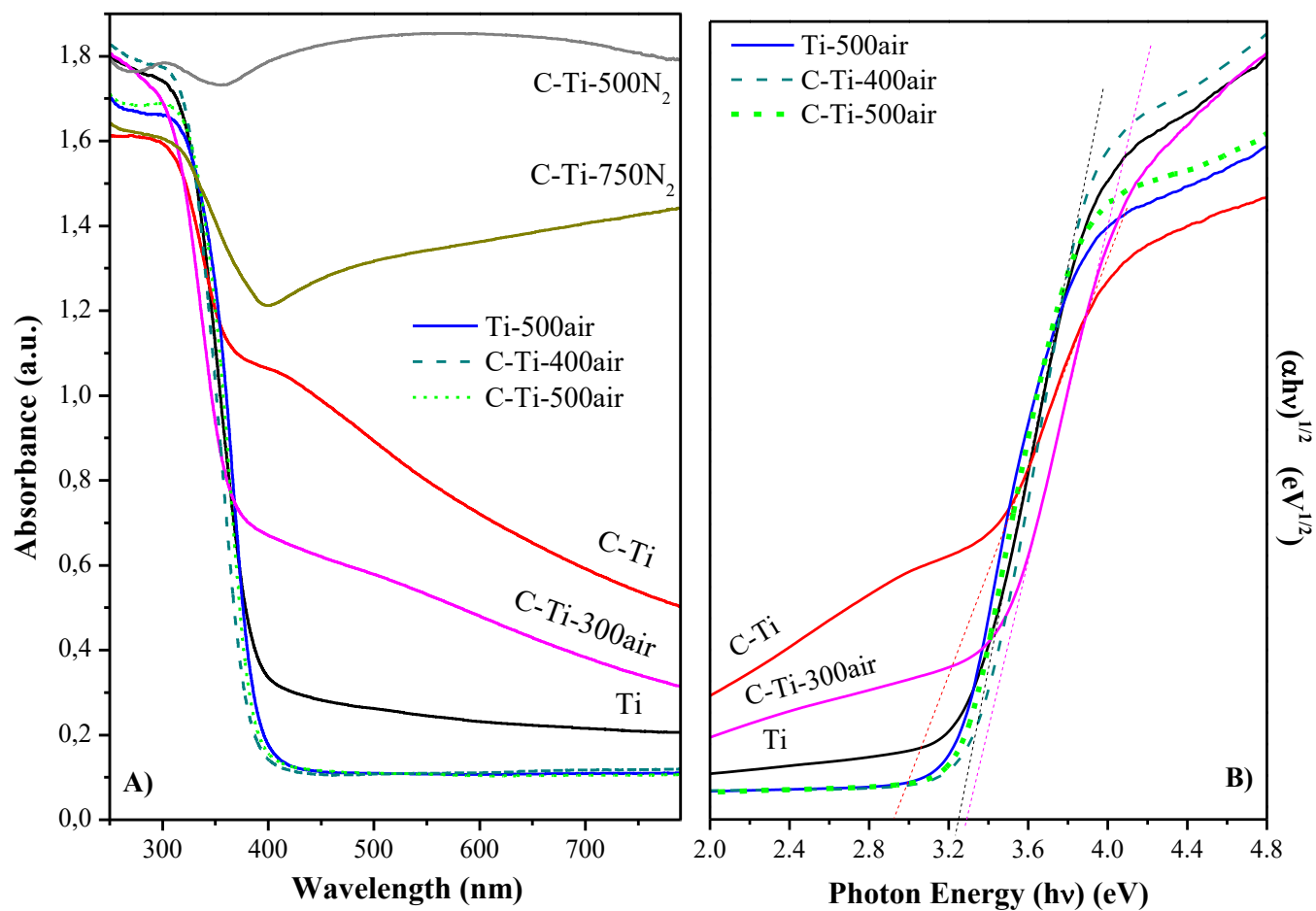


**Figure 5.** (A) UV-vis diffuse reflectance spectra and (B) the  $(\alpha h\nu)^{1/2}$  versus  $(h\nu)$  plot of the synthesized photocatalysts

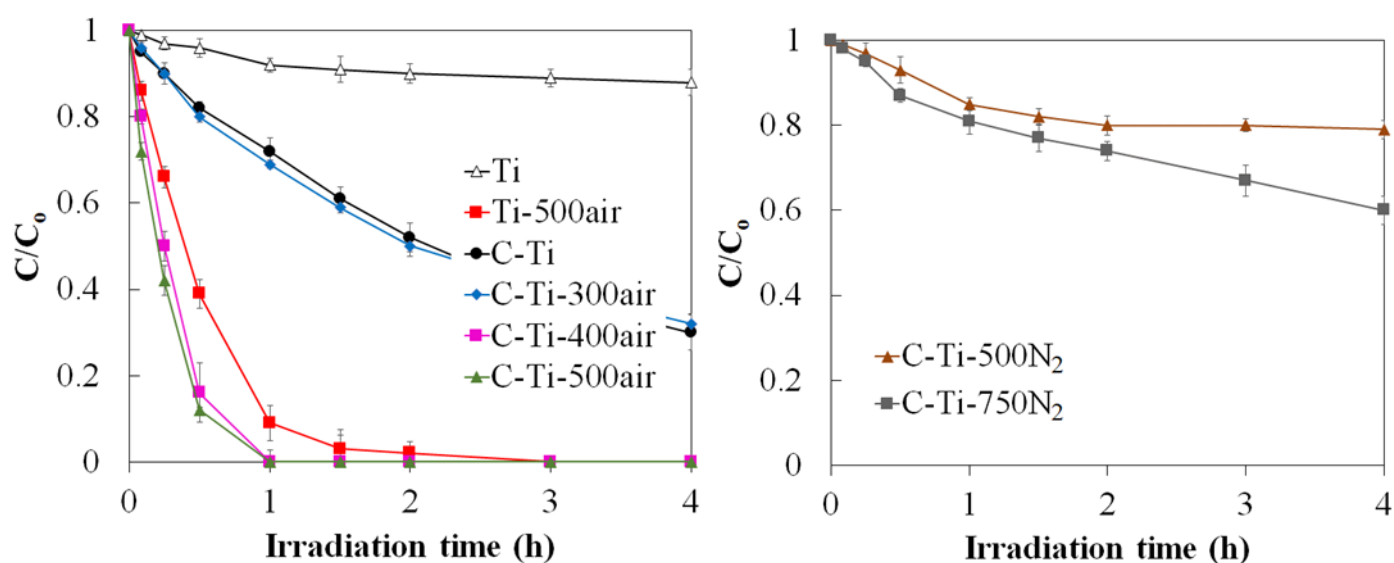


**Figure 6.** Time-course of acetaminophen concentration under solar irradiation with the synthesized photocatalysts (250 mg·L<sup>-1</sup> of catalyst; initial acetaminophen concentration: 5 mg·L<sup>-1</sup>; intensity of irradiation: 600 W·m<sup>-2</sup>).

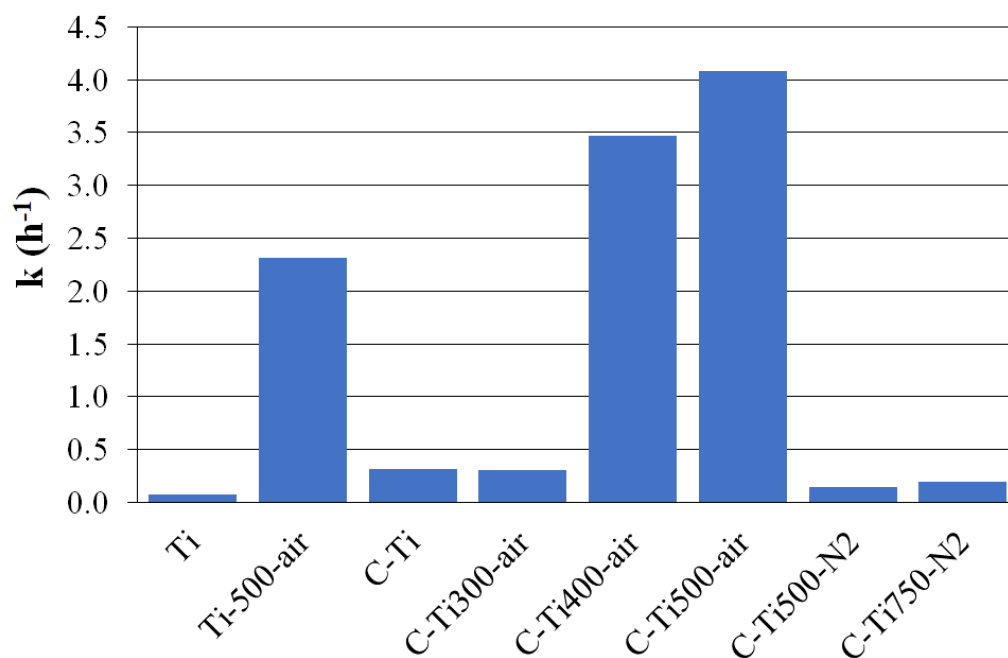


**Figure 7.** Apparent first order rate constant for acetaminophen disappearance.

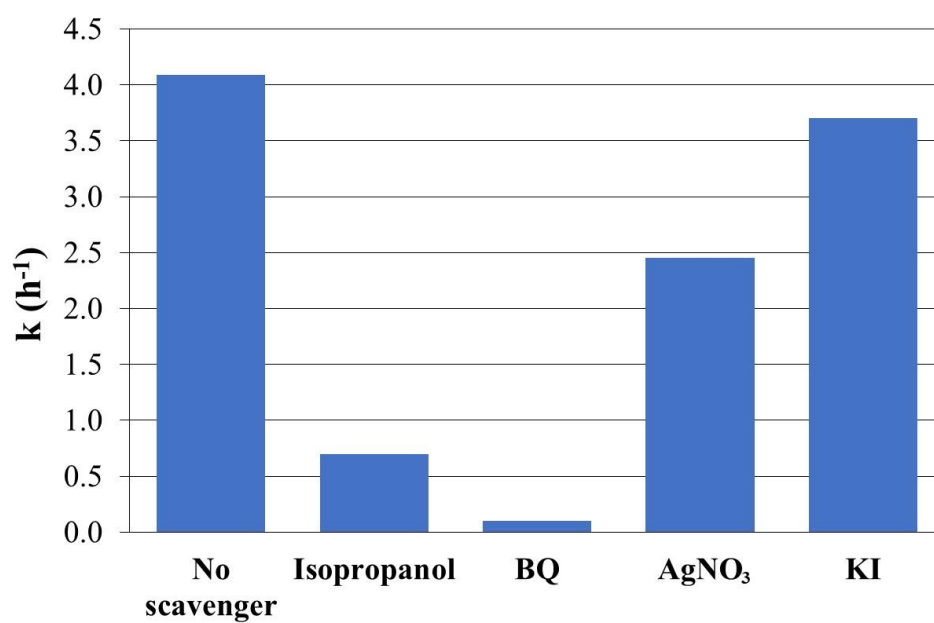


**Figure 8.** Apparent first order rate constant of acetaminophen degradation with C-Ti-500air in presence of different scavengers ( $[\text{ACE}] = 5 \text{ mg} \cdot \text{L}^{-1}$ ;  $[\text{scavenger}] = 0.06 \text{ M}$ ;  $[\text{photocatalyst}] = 250 \text{ mg} \cdot \text{L}^{-1}$ ; intensity of irradiation:  $600 \text{ W} \cdot \text{m}^{-2}$ ).

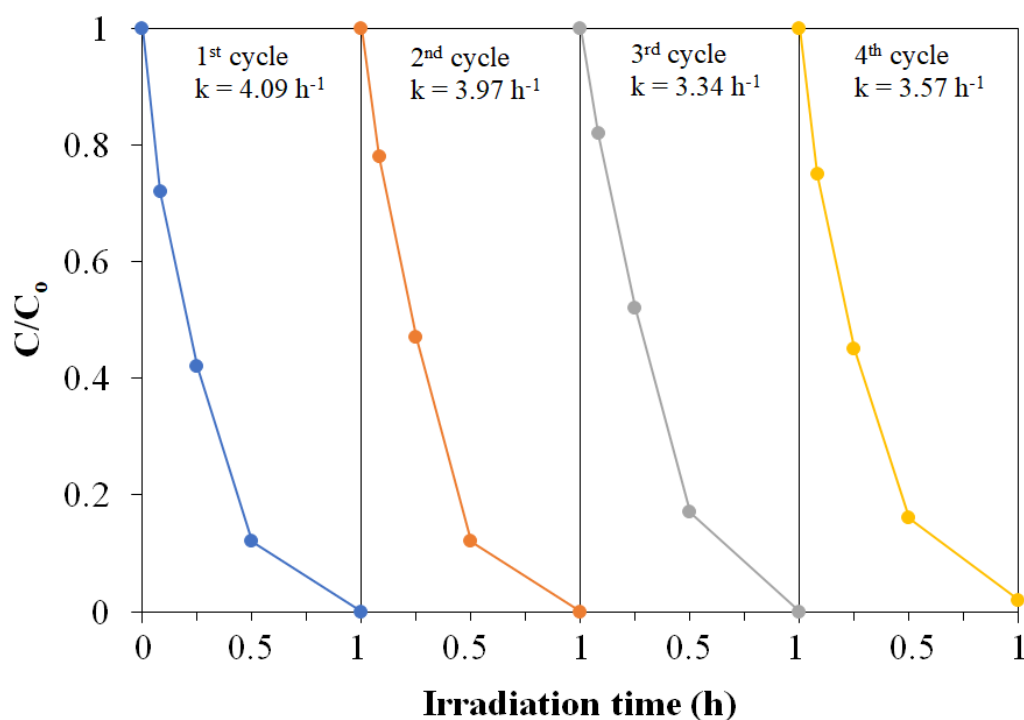


**Figure 9.** Performance of the C-Ti-500air photocatalyst upon successive cycles (same conditions than in Figure 6).

## Highlights

1. Novel C-modified TiO<sub>2</sub> photocatalysts were prepared by hydrothermal process
2. Lignin was used as carbonaceous precursor
3. The photocatalysts were tested for the degradation of acetaminophen
4. C-modified TiO<sub>2</sub> showed a higher degradation rate than non-modified TiO<sub>2</sub>
5. The photocatalysts showed good stability upon four successive cycles

[1] R. Fagan, D.E. McCormack, D.D. Dionysiou, S.C. Pillai, A review of solar and visible light active TiO<sub>2</sub> photocatalysis for treating bacteria, cyanotoxins and contaminants of emerging concern, *Mat. Sci. Semicon. Proc.* 42 (2016) 2–14.

- [2] A. Kubacka, M. Fernández-García, G. Colón, Advanced nanoarchitectures for solar photocatalytic applications, *Chem. Rev.* 112 (2012) 1555–1614.
- [3] J. Rivera-Utrilla, M. Sánchez-Polo, M.A. Ferro-García, G. Prados-Joya, R. Ocampo-Pérez, Pharmaceuticals as emerging contaminants and their removal from water. A review, *Chemosphere* 93 (2013) 1268–1287.
- [4] M.R. Hoffmann, S.T. Martin, W. Choi, D.W. Bahnemann, Environmental applications of semiconductor photocatalysis, *Chem. Rev.* 95 (1995) 69–96.
- [5] H. Dimitroula, V.M. Daskalaki, Z. Frontistis, D. I. Kondarides, P. Panagiotopoulou, N.P. Xekoukoulotakis, D. Mantzavinos, Solar photocatalysis for the abatement of emerging micro-contaminants in wastewater: Synthesis, characterization and testing of various TiO<sub>2</sub> samples, *Appl. Catal. B: Environ.* 117–118 (2012) 283–291.
- [6] A. Fujishima, X. Zhang, D.A. Trik, TiO<sub>2</sub> photocatalysis and related surface phenomena, *Surf. Sci. Rep.* 63 (2008) 515–582.
- [7] S.-Y. Lee, S.-J. Park, TiO<sub>2</sub> photocatalyst for water treatment applications, *J. Ind. Eng. Chem.* 19 (2013) 1761–1769.
- [8] M. Anpo, M. Takeuchi, The design and development of highly reactive titanium oxide photocatalysts operating under visible light irradiation, *J. Catal.* 216 (2003) 505–516.
- [9] L. Liu, X. Chen, Titanium dioxide nanomaterials: Self-structural modifications, *Chem. Rev.* 114 (2014) 9890–9918.
- [10] A. Di Paola, E. García-López, G. Marci, L. Palmisano, A survey of photocatalytic materials for environmental remediation, *J. Hazard. Mater.* 211–212 (2012) 3–29.
- [11] N. Serpone, A.V. Emeline, Semiconductor Photocatalysis: Past, Present, and Future Outlook, *J. Phys. Chem. Lett.* 3 (2012) 673–677.



- [12] S. Sakthivel, H. Kisch, Daylight photocatalysis by carbon-modified titanium dioxide, *Angew. Chem. Int. Ed.* 42 (2003) 4908–4911.
- [13] V. Etacheri, C. Di Valentin, J. Schneider, D. Bahnemann, S.C. Pillai, Visible-light activation of TiO<sub>2</sub> photocatalysts: advances in theory and experiments, *J. Photochem. Photobiol. C Photochem. Rev.* 25 (2015) 1–29.
- [14] Y. Choi, T. Umebayashi, M. Yoshikawa, Fabrication and characterization of C-doped anatase TiO<sub>2</sub> photocatalysts, *J. Mater. Sci.* 39 (2004) 1837–1839.
- [15] C. Di Valentin, G. Pacchioni, A. Selloni, Theory of carbon doping of titanium dioxide, *Chem. Mater.* 17 (2005) 6656–6665.
- [16] M. Pelaez, N.T. Nolan, S.C. Pillai, M.K. Seery, P. Falaras, A.G. Kontos, P.S.M. Dunlop, J.W.J. Hamilton, J.A. Byrne, K. O'Shea, M.H. Entezari, D.D. Dionysiou, A review on the visible light active titanium dioxide photocatalysts for environmental applications, *Appl. Catal. B: Environ.* 125 (2012) 331–349.
- [17] J. Chen, F. Qiu, W. Xu, S. Cao, H. Zhu, Recent progress in enhancing photocatalytic efficiency of TiO<sub>2</sub>-based materials, *Appl. Catal. A* 495 (2015) 131–140.
- [18] J. Fang, L. Xu, Z. Zhang, Y. Yuan, S. Cao, Z. Wang, L. Yin, Y. Liao, C. Xue, Au@TiO<sub>2</sub>–CdS ternary nanostructures for efficient visible-light-driven hydrogen generation, *ACS Appl. Mater. Interfaces* 5 (2013) 8088–8092.
- [19] M.D. Hernández-Alonso, S. García-Rodríguez, B. Sánchez, J. M. Coronado, Revisiting the hydrothermal synthesis of titanate nanotubes: new insights on the key factors affecting the morphology, *Nanoscale* 3 (2011) 2233–2240.
- [20] M.D. Hernández-Alonso, S. García-Rodríguez, S. Suarez, R. Portela, B. Sánchez, J.M. Coronado, Highly selective one-dimensional TiO<sub>2</sub>-based nanostructures for air treatment applications, *Appl. Catal. B: Environ.* 110 (2011) 251–259.



- [21] A.J. Maira, K.L. Yeung, C.Y. Lee, P.L. Yue, C.K. Chan, Fourier transform infrared study of the performance of nanostructured TiO<sub>2</sub> particles for the photocatalytic oxidation of gaseous toluene, *J. Catal.* 192 (2000) 185–196.
- [22] A.J. Maira, K.L. Yeung, J. Soria, J.M. Coronado, C. Belver, C.Y. Lee, V. Augugliaro, Gas-phase photo-oxidation of toluene using nanometer-size TiO<sub>2</sub> catalysts, *Appl. Catal. B Environ.* 29 (2001) 327–336.
- [23] J. Tauc, Absorption edge and internal electric fields in amorphous semiconductors, *Mater. Res. Bull.* 5 (1970) 721–726.
- [24] J. Zhang, P. Zhou, J. Liu, J. Yu, New understanding of the difference of photocatalytic activity among anatase, rutile and brookite TiO<sub>2</sub>, *Phys. Chem. Chem. Phys.* 16 (2014) 20382–20386.
- [25] R. Leary, A. Westwood, Carbonaceous nanomaterials for the enhancement of TiO<sub>2</sub> photocatalysis, *Carbon* 49 (2011) 741–772.
- [26] M. Thommes, K. Kaneko, A.V. Neimark, J.P. Olivier, F. Rodriguez-Reinoso, J. Rouquerol, K.S.W. Sing, *Pure Appl. Chem.* 87 (2015) 1051–1069.
- [27] H.-H. Ou, S.-L. Lo, Review of titania nanotubes synthesized via the hydrothermal treatment: Fabrication, modification, and application, *Separ. Purif. Tech.* 58 (2007) 179–191.
- [28] M.-S. Seo, H. Lee, Effect of calcination temperature on the lithiation capacities of carbon-coated titania nanotubes synthesized by anodization, *Elect. Mater. Lett.* 8 (2012) 259–262.
- [29] Z. Xiong, X.S. Zhao, Nitrogen-doped titanate-anatase core-shell nanobelts with exposed {101} anatase facets and enhanced visible light photocatalytic activity, *J. Am. Chem. Soc.* 134 (2012) 5754–5757.

- [30] Z. Jiang, W. Wei, D. Mao, C. Chen, Y. Shi, X. Lv, J. Xie, Silver-loaded nitrogen-doped yolk-shell mesoporous TiO<sub>2</sub> hollow microspheres with enhanced visible light photocatalytic activity, *Nanoscale* 7 (2015) 784–797.
- [31] W.J. Ren, Z.H. Ai, F.L. Jia, L.Z. Zhang, X.X. Fan, Z.G. Zou, Low temperature preparation and visible light photocatalytic activity of mesoporous carbon-doped crystalline TiO<sub>2</sub>, *Appl. Catal. B: Environ.* 69 (2007) 138–144.
- [32] Y.-T. Lin, C.-H. Weng, Y.-H. Lin, C.-C. Shiesh, F.-Y. Chen, Effect of C content and calcination temperature on the photocatalytic activity of C-doped TiO<sub>2</sub> catalyst, *Sep. Purifi. Technol.* 116 (2013) 114–123.
- [33] J. Shao, W. Sheng, M. Wang, S. Li, J. Chen, Y. Zhang, S. Cao, In situ synthesis of carbon-doped TiO<sub>2</sub> single-crystal nanorods with a remarkably photocatalytic efficiency, *Appl. Catal. B Environ.* 209 (2017) 311–319.
- [34] Q. Xiao, L. Ouyang, Photocatalytic activity and hydroxyl radical formation of carbon-doped TiO<sub>2</sub> nanocrystalline: Effect of calcination temperature, *Chem. Eng. J.* 148 (2009) 248–253.
- [35] J.F. Moulder, W.F. Stickle, P.E. Sobol, K.D. Bomben, in: J. Chastain, R.C. King, Jr. (Eds.), *Handbook of X-ray Photoelectron Spectroscopy*, Physical Electronics, Inc., Eden Prairie, MN, 1995.
- [36] Y. Zhang, Z. Zhao, J. Chen, L. Cheng, J. Chang, W. Sheng, C. Hu, S. Cao, C-doped hollow TiO<sub>2</sub> spheres: in situ synthesis, controlled shell thickness, and superior visible-light photocatalytic activity, *Appl. Catal. B: Environ.* 165 (2015) 715–722.
- [37] Z. Hua, Z. Dai, X. Bai, Z. Ye, H. Gu, X. Huang, A facile one-step electrochemical strategy of doping iron, nitrogen, and fluorine into titania nanotube arrays with enhanced visible light photoactivity, *J. Hazard. Mater.* 293 (2015) 112–121.

- [38] X. Wu, S. Yin, Q. Dong, C. Guo, H. Li, T. Kimura, T. Sato, Synthesis of high visible light active carbon doped TiO<sub>2</sub> photocatalyst by a facile calcination assisted solvothermal method, *Appl. Catal. B: Environ.* 142–143 (2013) 450–457.
- [39] A. Rey, P. García-Muñoz, M.D. Hernández-Alonso, E. Mena, S. García-Rodríguez, F.J. Beltrán, WO<sub>3</sub>–TiO<sub>2</sub> based catalysts for the simulated solar radiation assisted photocatalytic ozonation of emerging contaminants in a municipal wastewater treatment plant effluent, *Appl. Catal. B Environ.* 154–155 (2014) 274–284.
- [40] L. Liu, X. Chen, Titanium dioxide nanomaterials: self-structural modifications, *Chem. Rev.* 114 (2014) 9890–9918.
- [41] M. Henderson, A surface science perspective on TiO<sub>2</sub> photocatalysis, *Surf. Sci. Rep.* 66 (2011) 185–297.
- [42] Y. Liao, W. Que, Preparation and photocatalytic activity of TiO<sub>2</sub> nanotube powders derived by a rapid anodization process, *J. Alloys Compd.* 505 (2010) 243–248.
- [43] J. Zhang, P. Zhou, J. Liu, J. Yu, New understanding of the difference of photocatalytic activity among anatase, rutile and brookite TiO<sub>2</sub>, *Phys. Chem. Chem. Phys.* 16 (2014) 20382–20386.
- [44] C. Belver, J. Bedia, J.J. Rodriguez, Titania–clay heterostructures with solar photocatalytic applications, *Appl. Catal. B: Environ.* 176–177 (2015) 278–287.
- [45] C. Belver, J. Bedia, M.A. Álvarez-Montero, J.J. Rodriguez, Solar photocatalytic purification of water with Ce-doped TiO<sub>2</sub>/clay heterostructures, *Catal. Today* 266 (2016) 36–45.
- [46] C. Belver, J. Bedia, J.J. Rodriguez, Zr-doped TiO<sub>2</sub> supported on delaminated clay materials for solar photocatalytic treatment of emerging pollutants, *J. Hazard. Mater.* 322 (2017) 233–242.

- [47] M. Akkaria, P. Aranda, C. Belver, J. Bedia, A. Ben Haj Amara, E. Ruiz-Hitzky, ZnO/sepiolite heterostructured materials for solar photocatalytic degradation of pharmaceuticals in wastewater, *Appl. Clay Sci.* 156 (2018) 104–109.
- [48] M. Shafaei, E.K. Goharshadi, M. Mashreghi, M. Sadeghinia, TiO<sub>2</sub> nanoparticles and TiO<sub>2</sub>@graphene quantum dots nanocomposites as effective visible/solar light photocatalysts. *J. Photochem. Photobiol. A Chem.* 357 (2018) 90–102.
- [49] M. Pelaez, P. Falaras, V. Likodimos, K. O'Shea, A.A. de la Cruz, P.S.M. Dunlop, J.A. Byrne, D.D. Dionysiou, Use of selected scavengers for the determination of NF-TiO<sub>2</sub> reactive oxygen species during the degradation of microcystin-LR under visible light irradiation, *J. Mol. Catal. A* 425 (2016) 183–189.,
- [50] R. Palominos, J. Freer, M.A. Mondaca, H.D.J. Mansilla, Evidence for hole participation during the photocatalytic oxidation of the antibiotic flumequine, *Photochem. Photobiol.*, A 2008, 193, 139–145.
- [51] W. Li, D. Li, Y. Lin, P. Wang, W. Chen, X. Fu, Y. Shao, Evidence for the active species involved in the photodegradation process of methyl orange on TiO<sub>2</sub>, *J. Phys. Chem.* 116 (2012) 3552–3560.

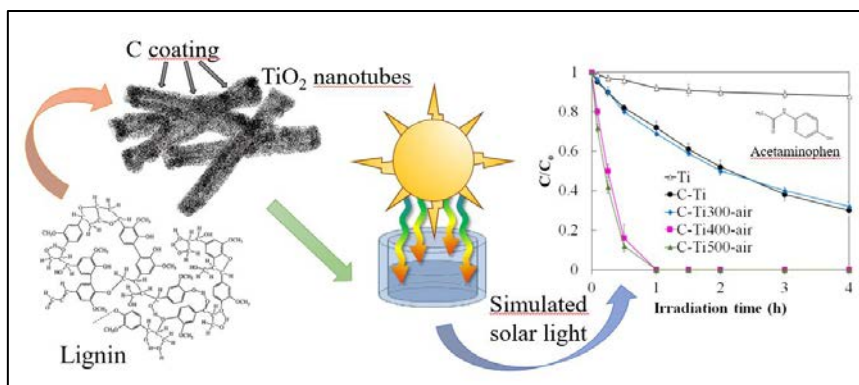


**Table 1.** C, H, N content and average crystal size of the synthesized photocatalysts.

Sample	%C	%H	%N	Average crystal size (nm) <sup>a</sup>
Ti-500air	---	---	---	21.7
C-Ti-300air	2.31	1.39	0.08	---
C-Ti-400air	0.32	0.77	0.04	11.8
C-Ti-500air	0.12	0.43	0.00	17.0
C-Ti-500N <sub>2</sub>	5.85	0.79	0.04	11.0
C-Ti-750N <sub>2</sub>	2.97	0.17	0.03	29.6

<sup>a</sup> Anatase crystal size estimated from (101) reflection peak**Table 2.** Porous texture and band gap values (E<sub>g</sub>) of the photocatalysts.

Sample	S <sub>BET</sub> (m <sup>2</sup> ·g <sup>-1</sup> )	S <sub>EXT</sub> (m <sup>2</sup> ·g <sup>-1</sup> )	V <sub>pore</sub> (cm <sup>3</sup> ·g <sup>-1</sup> )	E <sub>g</sub> (eV)
Ti	327	309	1.20	3.25
Ti-500air	106	100	0.54	3.12
C-Ti	342	329	1.13	2.95
C-Ti-300air	323	300	1.29	3.28
C-Ti-400air	147	138	0.87	3.25
C-Ti-500air	111	102	0.90	3.18
C-Ti-500N <sub>2</sub>	195	195	0.90	---
C-Ti-750N <sub>2</sub>	73	56	0.34	---

**Table 3.** Surface elemental composition (at., %) of the photocatalysts as obtained by XPS.

Muestra	%Ti	%O	%C	O/Ti
Ti-500air	28.3	63.4	8.3	2.24
C-Ti-500air	28.5	63.9	7.8	2.24
C-Ti-500N <sub>2</sub>	21.7	50.9	27.4	2.35

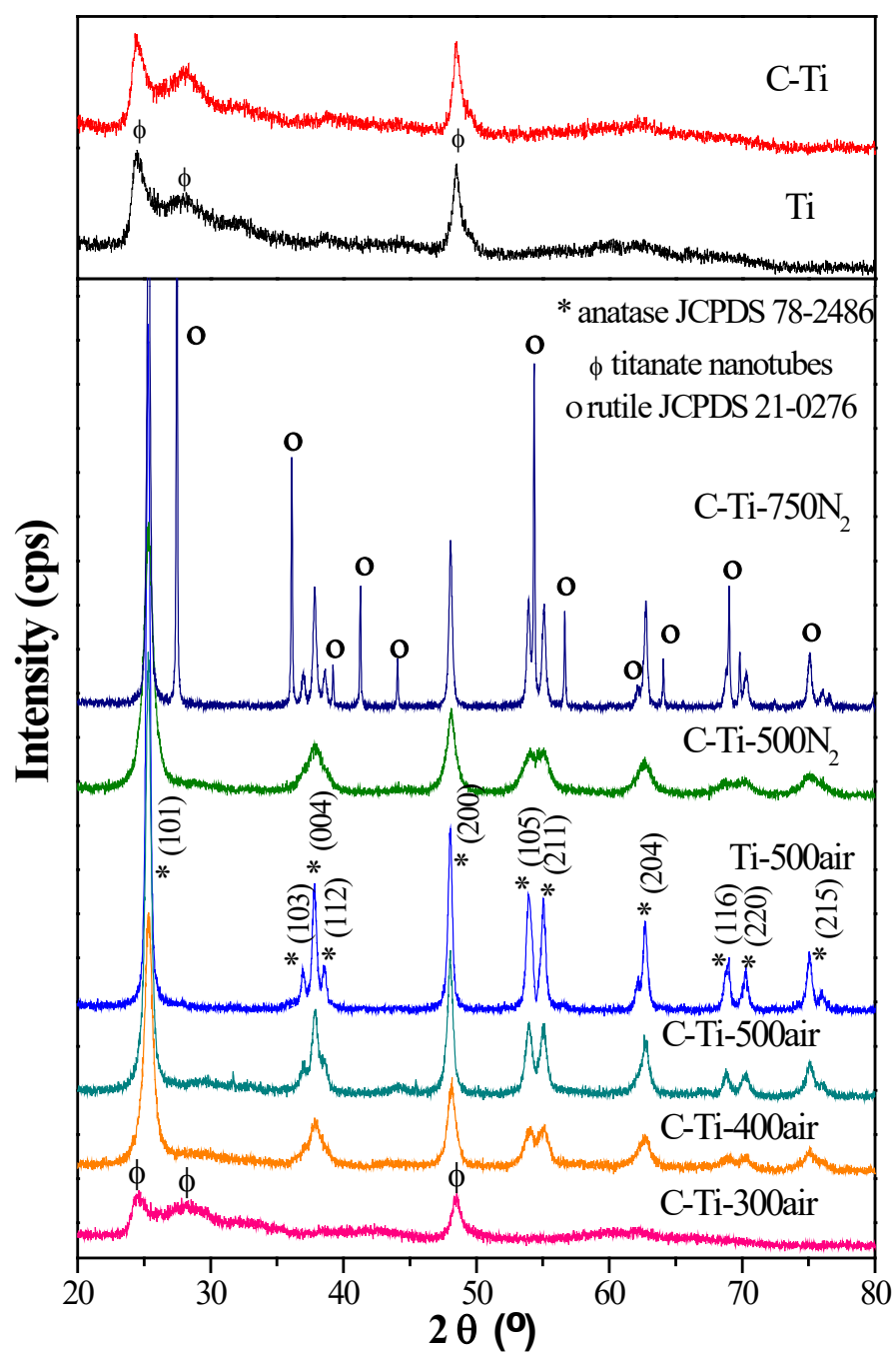


**Figure 1.** XRD patterns of Ti and C-Ti samples from hydrothermal synthesis and the resulting from further heat treatment under different conditions.

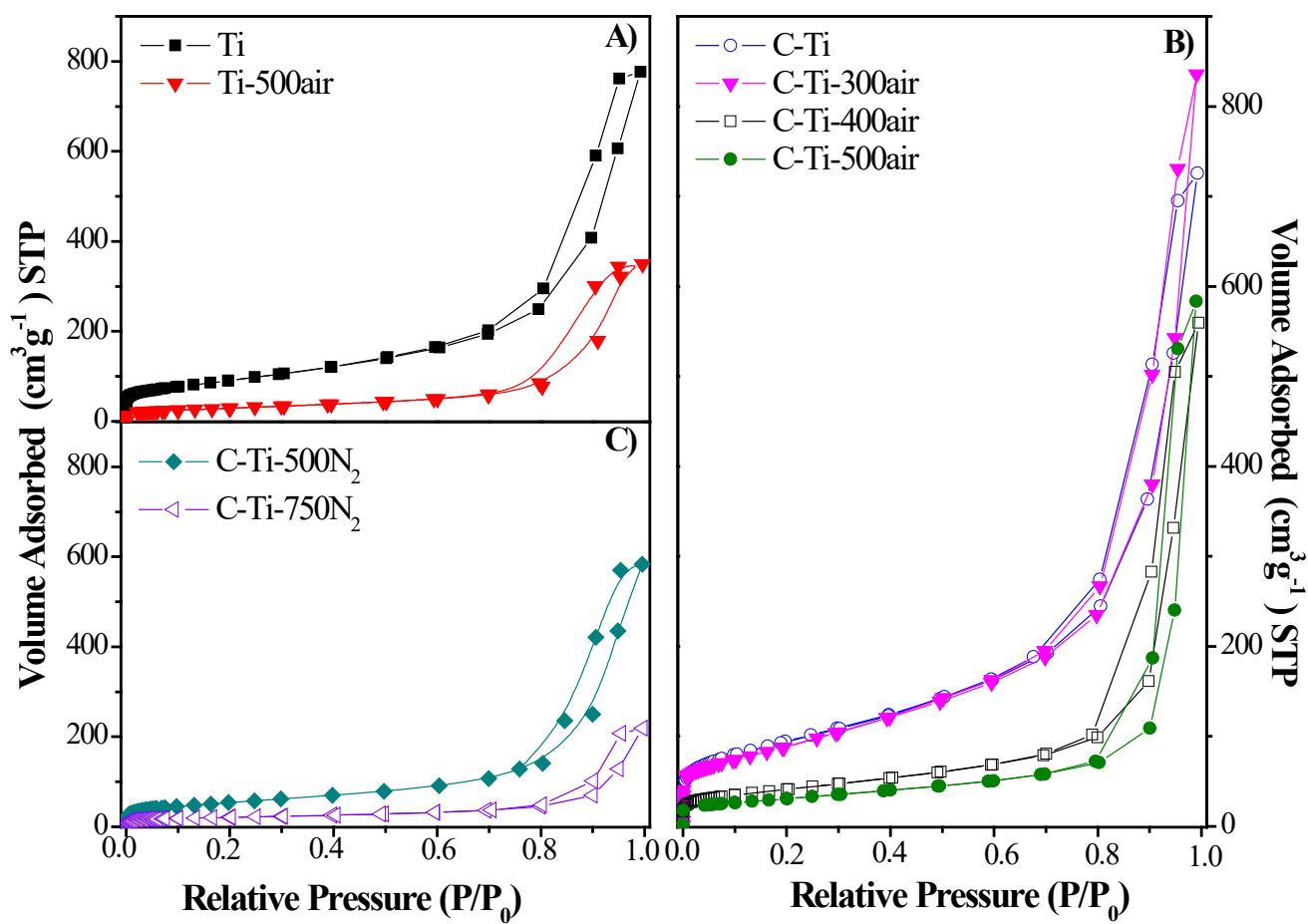


**Figure 2.** N<sub>2</sub> adsorption-desorption isotherms of the synthesized photocatalysts



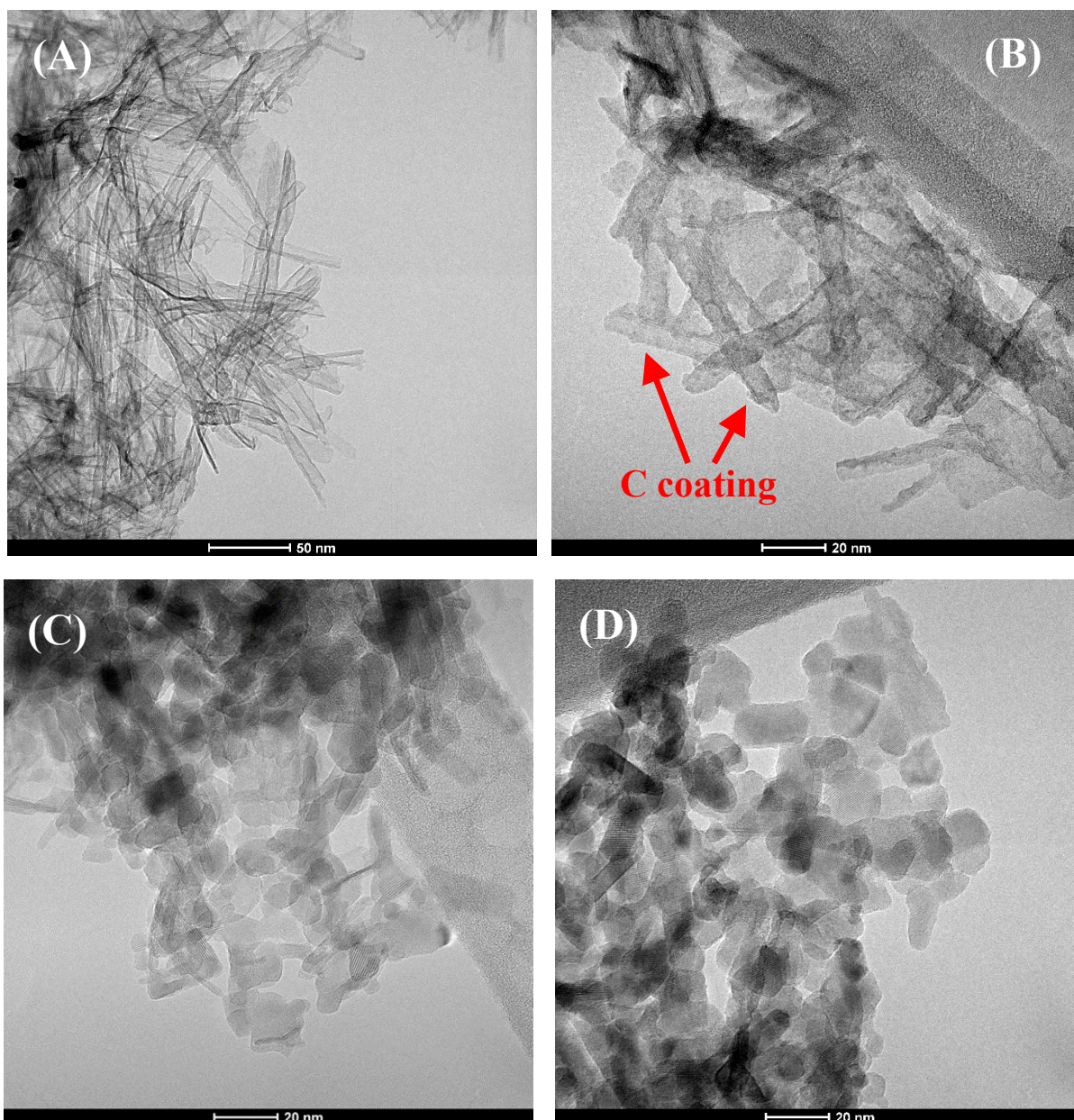


**Figure 3.** TEM images of (A) Ti, (B) C-Ti, (C) Ti-500air and (D) C-Ti-500air

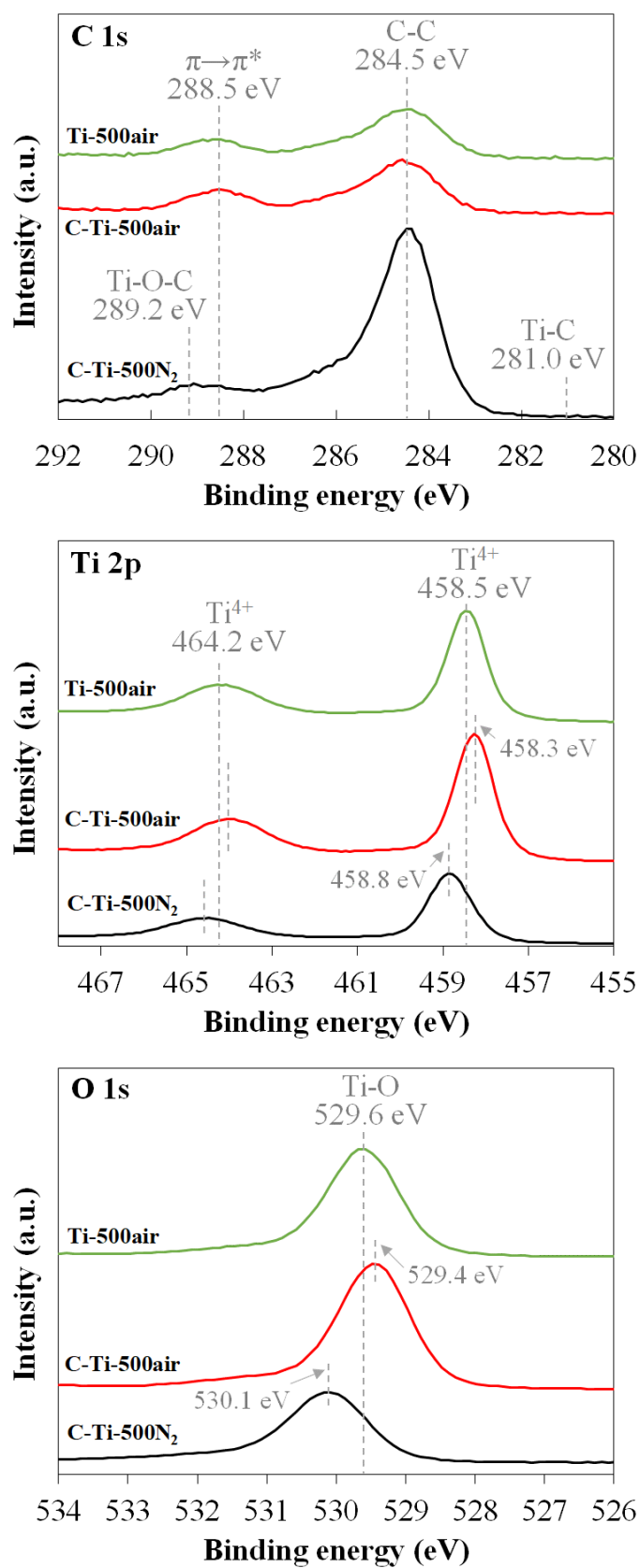


**Figure 4.** C 1s, Ti 2p and O 1s XPS high-resolution spectra of Ti-500air, C-Ti-500air and C-Ti-500N<sub>2</sub>

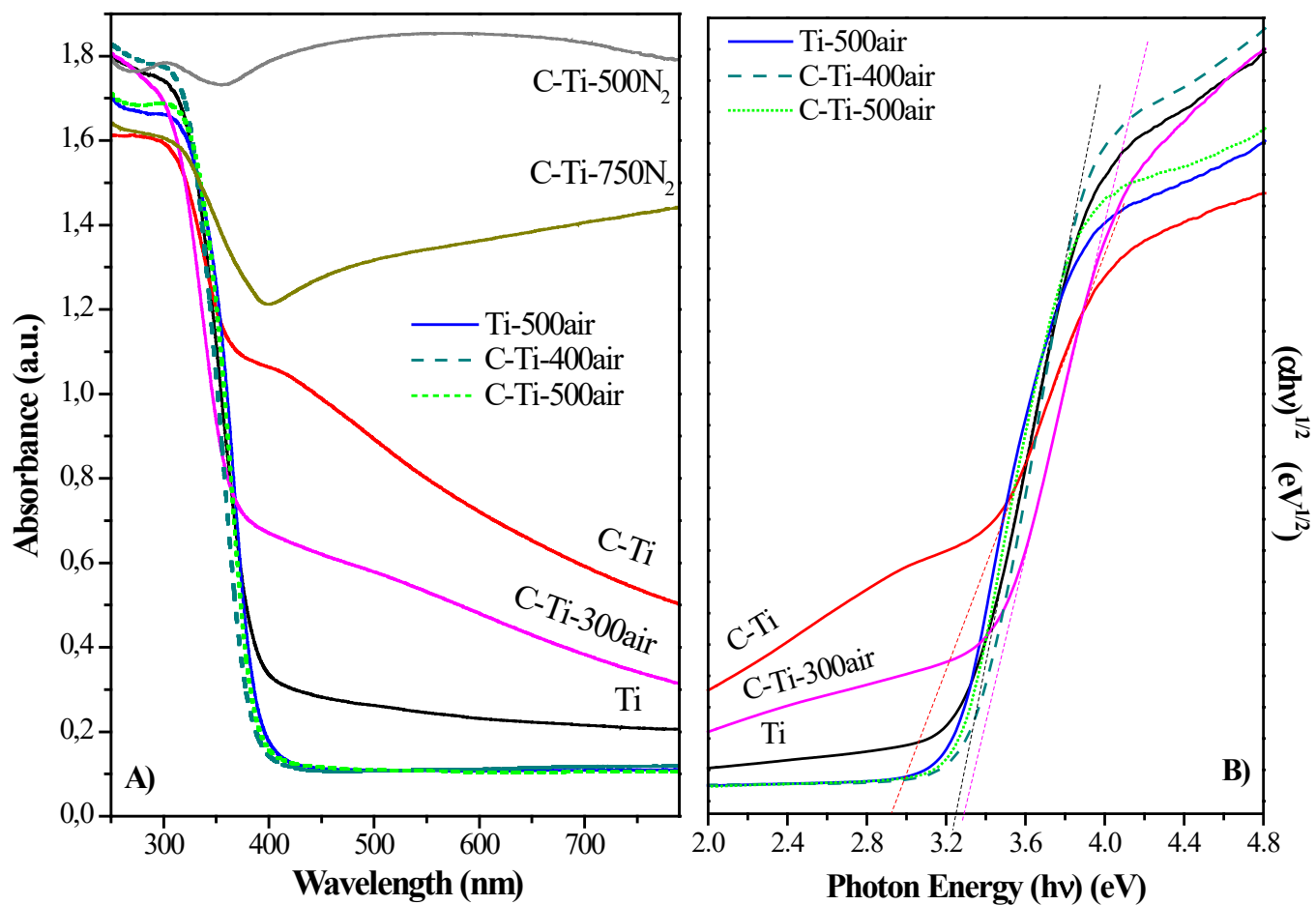


**Figure 5.** (A) UV-vis diffuse reflectance spectra and (B) the  $(F(R) \cdot hv)^{1/2}$  versus  $(hv)$

plot of the synthesized photocatalysts

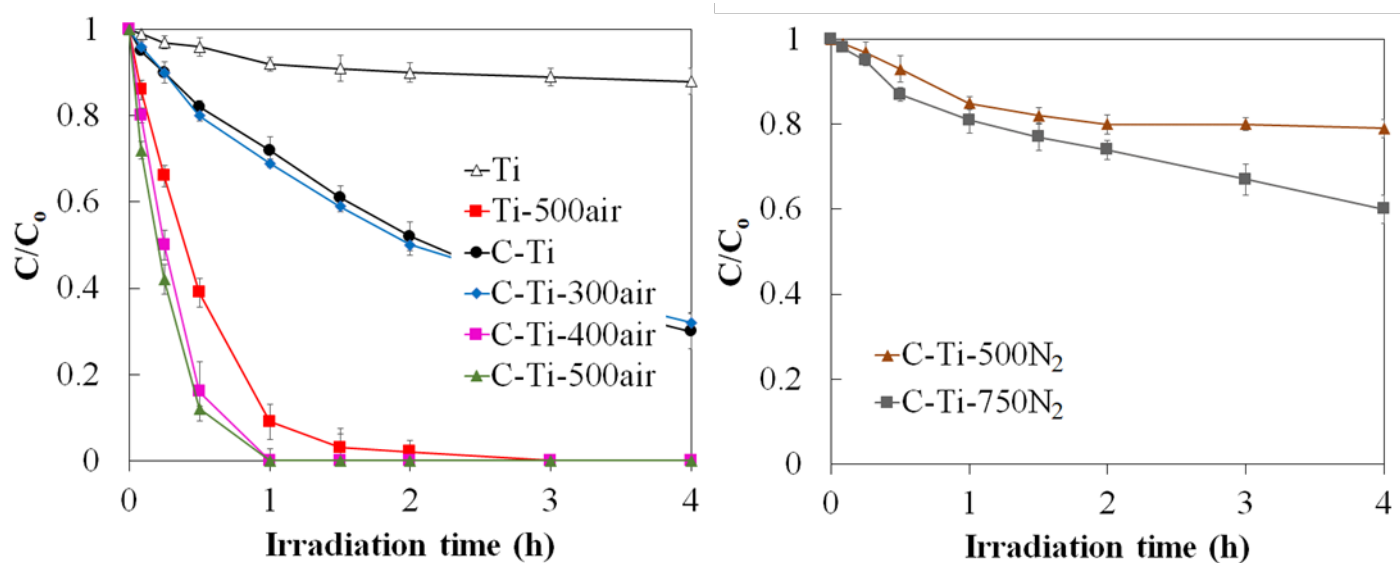


**Figure 6.** Time-course of acetaminophen concentration under solar irradiation with the synthesized photocatalysts (250 mg·L<sup>-1</sup> of catalyst; initial acetaminophen concentration: 5 mg·L<sup>-1</sup>; intensity of irradiation: 600 W·m<sup>-2</sup>).

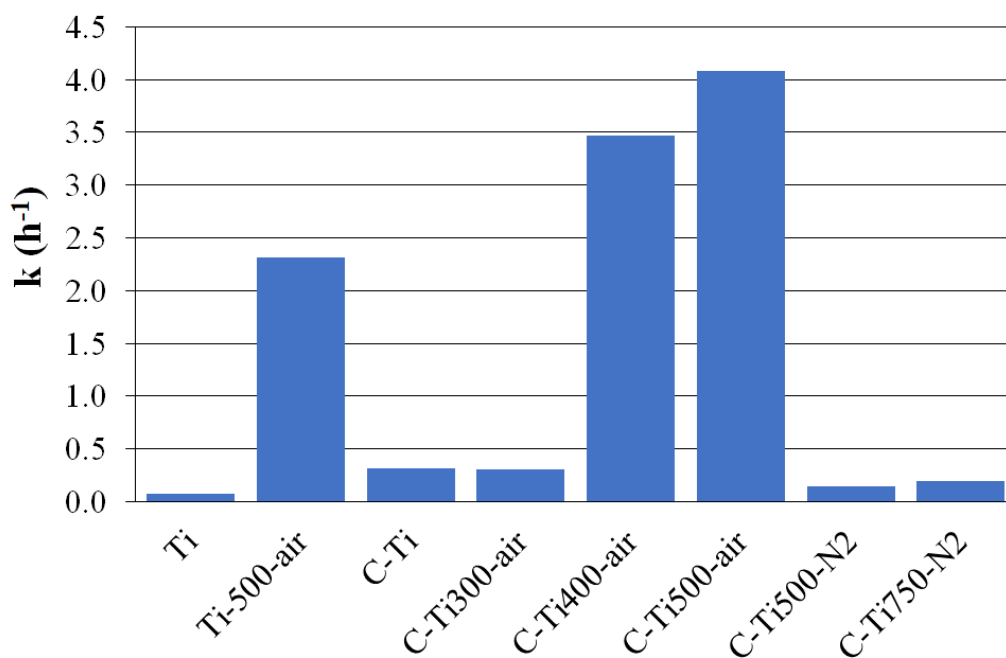


**Figure 7.** Apparent first order rate constant for acetaminophen disappearance.

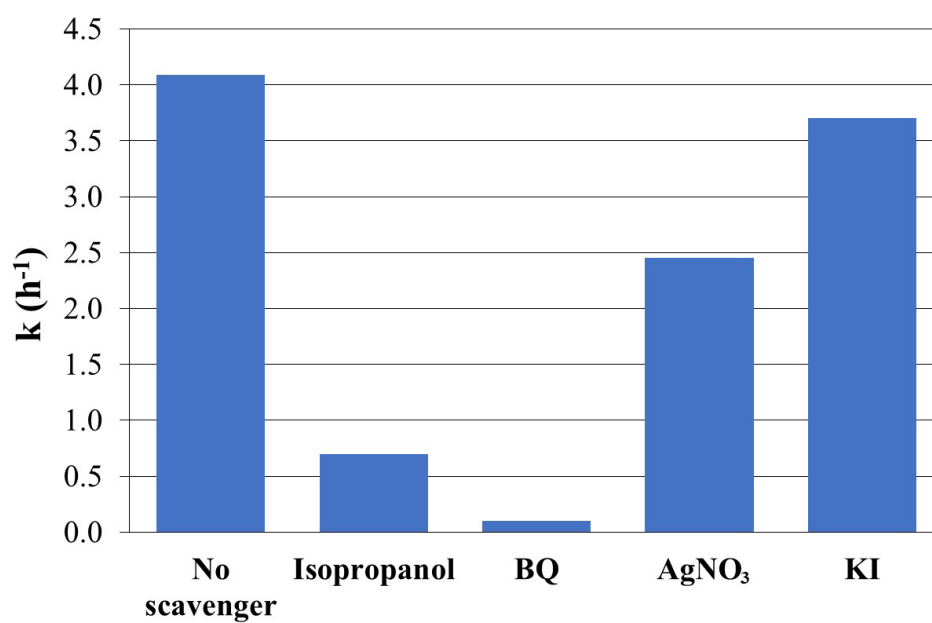


**Figure 8.** Apparent first order rate constant of acetaminophen degradation with C-Ti-500air in presence of different scavengers ( $[\text{ACE}] = 5 \text{ mg}\cdot\text{L}^{-1}$ ;  $[\text{scavenger}] = 0.06 \text{ M}$ ;  $[\text{photocatalyst}] = 250 \text{ mg}\cdot\text{L}^{-1}$ ; intensity of irradiation:  $600 \text{ W}\cdot\text{m}^{-2}$ ).

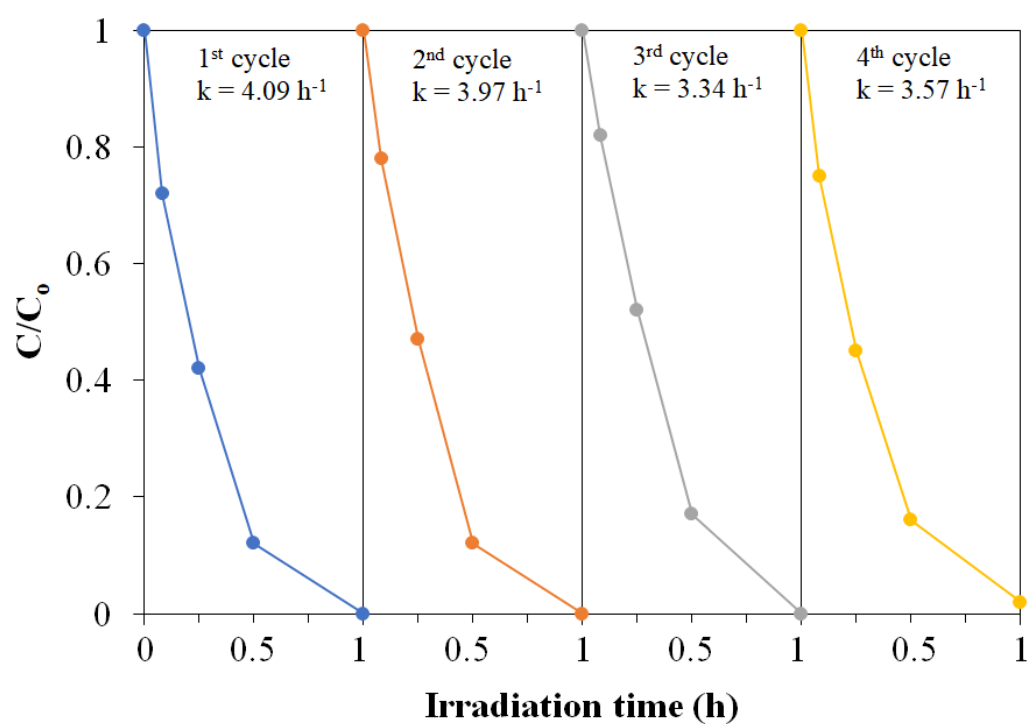


**Figure 9.** Performance of the C-Ti-500air photocatalyst upon successive cycles (same conditions than in Figure 6).